THE ASTROPHYSICAL JOURNAL, 319:850–867, 1987 August 15

CONDITIONS FOR THE FORMATION OF MASSIVE STARS

MARK G. WOLFIRE AND JOSEPH P. CASSINELLI
Washburn Observatory, University of Wisconsin-Madison
Received 1986 October 21; accepted 1987 February 5

ABSTRACT

Upper limits on the masses of stars that can form are reinvestigated, and models for the inflow of matter through cocoons around stars of 60, 100, and 200 $M_\odot$ are calculated. Radiative forces on dust play a crucial role in halting an accretion inflow. We consider rather general conditions that must hold at the inner and outer boundaries of a protostellar cocoon. Limits are derived on the dust-to-gas ratios and mass inflow rates that will permit inflow onto very massive stars. It is found that the ISM dust mixture of Mathis, Rumpl, and Nordsieck does not allow an inflow to occur. It is necessary that the standard Galactic gas-to-dust ratio be reduced by a factor of 4 or more and the larger graphite grains be missing from the dust distribution function. The inflows also require mass accretion rates of $\sim 10^{-3}\ M_\odot\ \mathrm{yr}^{-1}$ or more for there to be sufficiently strong ram pressure to overcome the strong radiative deceleration that occurs at the inner boundary of the shell. For the model calculations, radiative deceleration of grains and grain destruction processes are explicitly accounted for in an iterative solution of the radiation and hydrodynamic equations. Inflow can occur if intermediate-sized grains (0.05–0.25 μm) are missing from the initial gas/dust mixture. Very small grains or very large grains (>100 μm) allow infall to proceed. The existence of massive stars in certain locations in galaxies suggest that preconditioning of the interstellar medium by shocks or by turbulence is required for massive star formation.

Subject headings: stars: formation — stars: interiors — stars: massive

I. INTRODUCTION

There is a conflict between the observational and current theoretical estimates of the most massive stars. The location in the H-R diagram of stars in the Galaxy and in the LMC indicate that some stars with masses of 100 $M_\odot$ or more exist (de Jager 1980; Humphreys and McElroy 1984). Even with the high spatial resolution observations of Weigelt and Baier (1985), it is possible that objects of masses as high as 250 $M_\odot$ are present in R136a (although certainly less massive than the 750–2000 $M_\odot$ range proposed by Feitzinger *et al.* 1980 and Chu, Cassinelli, and Wolfire 1984). The progenitor of SN 1961v in NGC 1058 is estimated to have been over 1000 $M_\odot$ (Utrobin 1984). However, there are theoretical arguments indicating that stars more massive than ~ 40–100 $M_\odot$ cannot form (Larson and Starrfield 1971; Kahn 1974; Yorke and Krügel 1977). It is important, therefore, to investigate these limits on star formation.

The calculations of Bodenheimer and Sweigart (1968), Larson (1969), Shu (1977), and others have established that the early phases of collapse for a nonrotating protostellar cloud proceeds nonhomologously. The central regions rapidly form a core, while the surrounding dust-gas envelope continues to fall inward. If the core is massive enough, then hydrogen burning will begin in the interior while it continues to build up mass by accreting the surrounding cloud (Appenzeller and Tscharnuter 1974). Larson and Starrfield (1971) and Kahn (1974) proposed that radiation pressure acting on grains in the inflow will halt the infall of material and thereby limit the total mass accumulated by the protostar. Kahn's result was that a core of 40 $M_\odot$ had sufficient luminosity to stop the accretion; however, he emphasized that the limit was sensitive to the assumed grain properties and abundances.

Since Kahn's analysis there have been major advances in the understanding of interstellar grain properties. Mathis, Rumpl, and Nordsieck (1977, hereafter MRN), proposed a grain model that fits many of the observed properties of interstellar extinction. It is now realized that any acceptable interstellar extinction model must consist of a distribution in grain sizes of at least two compositions (Fitzpatrick and Massa 1987). Star formation calculations, however, have thus far accounted for only a single grain size, with some analyses including the possibility of an icy mantle. Grain destruction processes have also been studied for the general interstellar environment by Barlow (1978), Shull (1978), Draine (1979), Draine and Salpeter (1979*b*), and Seab and Shull (1983). The destruction of grains in protostellar dust shells has been considered by Burke and Silk (1976) and Stahler, Shu, and Taam (1981). However, there have been no investigations on the effects of grain destruction in determining the maximum mass that a growing protostar may accumulate.

In this paper we reevaluate the previous theoretical mass limits in light of the better understanding of grain properties that is now available. We estimate conditions necessary for the formation of massive stars. We also construct a numerical model of the accretion inflow, accounting for the modification of the grain mixture due to destruction processes. The model calculations require the solution of coupled radiation transfer and radial, steady state hydrodynamic equations. The radiation transfer procedure has previously been discussed by Wolfire and Cassinelli (1986, hereafter WC1).

In § II we describe the basic structure of a protostellar accretion flow. In § III we discuss the stellar mass limit proposed by Kahn (1974). We review the optical properties of grains in § IV. In § V we discuss general requirements for massive star formation by a consideration of the boundary conditions. We describe our numerical calculations of an accretion flow in § VI and present the results in § VII. Section VIII is a summary and discussion of our analysis.

II. STRUCTURE OF A PROTOSTELLAR CLOUD

The nonhomologous collapse of a protostellar cloud creates a small hydrostatic core. The core acquires mass by accreting the surrounding envelope of gas and dust during a period known as the main accretion phase (Stahler, Shu, and Taam 1980). Dust grains in the inflow are destroyed within some dust destruction radius leaving a dust shell or cocoon surrounding the core. Within this radius the flow consists of inflowing gas, while beyond this radius the flow consists of inflowing gas and dust. As we show in this paper, grains are not all destroyed at a single radius; rather, grains are destroyed at radial distances that depend on their size and composition and on the dominant destruction mechanism acting in the inflow. Stahler, Shu, and Taam (1980, 1981) describe the envelope structure of a low-mass protostar. They trace the evolution of a 0.01 $M_\odot$ core and its surrounding cloud through the main accretion phase to the formation of a 1 $M_\odot$ star. Yorke (1979) considered the evolution of more massive clouds of initial masses of 3 $M_\odot$ and 10 $M_\odot$.

During the accretion phase, the low-mass core luminosity is mainly produced by an accretion shock. The shock is a result of the rapid deceleration of infalling gas at the surface of the hydrostatic core, and the shock luminosity may be as high as $L_{sh} = GM_* \dot{M}/R_*$, where $\dot{M}$ is the inflow rate, M_* is the core mass, and R_* is the core radius (see Winkler and Newman 1980 and Stahler, Shu, and Taam 1980 for a discussion of the accretion shock). For higher mass cores, thermonuclear energy generation turns on while the core is accreting material. In this case the total luminosity consists of both a nuclear-burning component, L^*, and shock luminosity, L_{sh}.

If the accretion rate is high enough, the flow becomes optically thick prior to reaching the core. In this case an effective photosphere forms with an effective temperature somewhat cooler than that of a core-mass zero-age main-sequence star. For massive cores an H II region is present beyond the effective photosphere. The infall of material keeps the H II region compact, much smaller in radial extent than the shell. See WC1 and Yorke (1984) for discussions of the effective photosphere and compact H II region surrounding massive cores.

The outer regions of the dust shell are diffuse and smoothly join the surrounding molecular cloud; therefore, the radius of the outer "boundary" of the shell is somewhat arbitrary. In practice the chosen definition of the boundary depends on the method of analysis. Stahler, Shu, and Taam (1980) adopted the definition that the outer shell boundary is the radius at which the Planck mean optical depth becomes equal to unity. This defines a dust photosphere characterized by a single radius and temperature. Yorke (1979) assumes that the outer boundary is that of the initial gravitationally unstable cloud. In our calculations we choose to simply select the outer boundary to be the point at which the shell densities are comparable to those in dense molecular clouds $\sim 10^{-19}$ g cm^{-3}. This is also the density of the initial cloud in the calculations of Larson (1969).

III. THE KAHN LIMIT TO STELLAR MASSES

Kahn (1974) found an analytic solution to the velocity structure of a protostellar accretion flow. His solution accounts for the deceleration of the inflow because of the radiative forces on the grains. The ultraviolet and visible radiation from the core is assumed to be absorbed in a thin shell at the inner edge of the dust cocoon with the grains then reradiating this energy in the infrared. In Kahn's model, the radiation pressure gradient of the IR field decelerates grains in the inflow. The outward momentum flux absorbed by the grains is transferred by collisions to the gas. The drag forces thereby decelerate the inward flow of gas. At some point in the inflow, the grains could become hot enough to be destroyed by sublimation, where heating is produced by both the direct stellar field and the diffuse IR shell field. If the inward flow can be maintained through the grain destruction region, then accretion will continue since radiation pressure will no longer be able to halt the flow. If, on the other hand, the flow is stopped before grains can be destroyed, then accretion is halted and the core is considered to have reached its final mass. In Kahn's solution, when the core luminosity-to-mass ratio, L/M, exceeds $\sim 10^4$ ergs s^{-1} g^{-1} the inflow of material is reversed. This L/M ratio corresponds, in our Galaxy, to a maximum core mass of ~ 40 $M_\odot$. A value for the maximum stellar mass which is widely quoted. Kahn showed, however, that the maximum L/M ratio, derived from his analysis, is inversely proportional to the grain opacity. Regions of lower grain-to-gas mass ratios would therefore form more massive stars, and the stellar upper mass limit is in fact a sensitive function of the particular grain properties of a star-forming region.

In our reanalysis of Kahn's work we find that the maximum L/M ratio is proportional to T_{sub}^{-3}, where T_{sub} is the assumed temperature at which grains sublimate. In Kahn's derivation in which the maximum stellar mass is ~ 40 $M_\odot$, he assumed a sublimation temperature of 3670 K. This rather high temperature is the sublimation temperature of graphite at standard pressure. However, the laboratory data indicate that in the low-pressure environment of star formation, graphite sublimates at much lower temperatures (see discussions by Salpeter 1974, 1977). We find that if the sublimation temperature is decreased to 2000 K, the maximum L/M ratio derived from Kahn's analysis corresponds to ~ 1000 $M_\odot$ core. Figure 1 shows the dependence of the maximum L/M ratio on the sublimation temperature. The reason the mass limit depends inversely on the grain sublimation temperature can be understood qualitatively by considering the radiative acceleration on grains in the outer regions of the cocoon. The radiative acceleration is proportional to the product of the opacity times the radiative flux, kF. Except for a narrow region near the inner

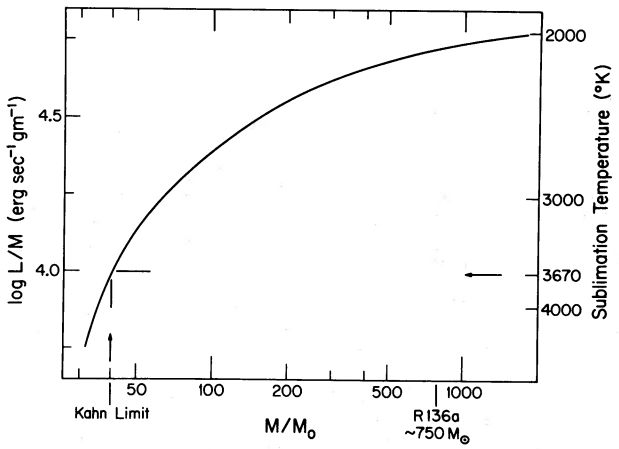

FIG. 1.—Relation between the Kahn upper mass limit and the dust sublimation temperature. Decreasing the sublimation temperature allows the core to have a larger L/M and a correspondingly larger mass. The sublimation temperature of ~ 3600 K, assumed by Kahn, allows a maximum L/M of $\sim 10^4$ ergs s^{-1} g^{-1} or a core mass of ~ 40 $M_\odot$.

boundary of the cocoon, the radiation field is reradiated dust emission. The lower the dust sublimation temperature, the softer this radiation field will be. Since the opacity is lower at larger wavelengths ($k \propto \lambda^{-2}$ in Kahn's analysis), the product of kF tends to be lower in a softer radiation field. This simple picture explains much of the general behavior seen in Figure 1. On the other hand, as stated earlier, Kahn's maximum L/M is also inversely proportional to the grain opacity. His adopted mean opacity is a factor of ~ 7 lower than expected from MRN grains in a Planckian radiation field of $T = 1000$ K. This underestimate of opacity is in part responsible for the maximum core mass reaching $\sim 1000\ M_\odot$ when grain sublimation temperatures are decreased. In § VII of this paper we will see important effects associated with a more thorough treatment of the radiation field and grain opacities in an accretion flow. The net effect will be to reduce the upper limit to well below $1000\ M_\odot$ again.

IV. OPTICAL PROPERTIES OF GRAINS

Since grains play such an important role in the star formation process, we review here the quantities used in deriving the opacity from a collection of grains. More complete descriptions of grain properties and opacities are given by WC1, Draine and Lee (1984, hereafter DL), and Bohren and Huffman (1983). The absorption and scattering cross sections to radiation of wavelength λ presented by a single grain is represented by the products:

$$C_\lambda^A = \pi a^2 Q^A(a, \lambda)\,, \tag{1}$$

$$C_\lambda^S = \pi a^2 Q^S(a, \lambda)\,, \tag{2}$$

$$C_\lambda^T = C_\lambda^A + C_\lambda^S\,, \tag{3}$$

where a is the grain radius and Q^A and Q^S are the absorption and scattering efficiencies. The efficiencies are a function of the grain composition, grain size, and the wavelength of the incident radiation field. Given the wavelength-dependent complex indices of refraction for a particular grain composition, Mie theory can be used to calculate Q^A and Q^S as discussed in WC1 and DL.

For a collection of grains the mass absorption coefficient is defined as

$$\kappa_\lambda = \sum_i \int_{a_-^i}^{a_+^i} n_i(a)\pi a^2 Q^A(a, \lambda)\,\frac{X}{m_H}\,da\,, \tag{4}$$

where the sum is taken over all grain compositions i, a_-, and a_+, are the minimum and maximum grain sizes, $n_i(a)$ is the number of grains per hydrogen atom in the range a to $a + da$, X is the local mass fraction of hydrogen (assumed $= 0.7$), and m_H is the mass of hydrogen. The scattering opacity is calculated in a similar way by substituting Q^S in place of Q^A. A selection of the grain composition, a_+, a_-, and $n_i(a)$ defines a complete grain model.

Since we are interested in the dynamical effects caused by grains, we also need the radiation pressure cross section that is used in calculating the transfer of momentum from the radiation field to the grains. We represent this efficiency by Q^{pr} given by

$$\pi a^2 Q^{pr}(a, \lambda) = \pi a^2[Q^A(a, \lambda) + (1 - g_\lambda)Q^S(a, \lambda)]\,, \tag{5}$$

where g_λ is the cosine of the scattering angle. For complete forward scattering $g_\lambda = 1$, and for isotropic scattering $g_\lambda = 0$. The term $1 - g_\lambda$ accounts for the decrease in momentum transfer due to forward scattered photons. The radiation pressure coefficient per gram of gas resulting from the collection of grains is

$$k_\lambda^{pr} = \sum_i \int_{a_-^i}^{a_+^i} n_i(a)\pi a^2 Q^{pr}(a, \lambda)\,\frac{X}{m_H}\,da\,. \tag{6}$$

We also make use of the flux mean radiation pressure cross section:

$$C_H^{pr} = \pi a^2 Q_H^{pr} = \int_0^\infty \pi a^2 Q^{pr}(a, \lambda) H_\lambda\, d\lambda / H\,, \tag{7}$$

and flux mean radiation pressure coefficient:

$$k_H^{pr} = \int_0^\infty k_\lambda^{pr} H_\lambda\, d\lambda / H\,, \tag{8}$$

where H_λ is the first angular moment of the monochromatic intensity:

$$H_\lambda = \frac{L_\lambda(r)}{(4\pi r)^2} = \frac{1}{2}\int_{-1}^{+1} I(\mu, r)\mu d\mu\,, \tag{9}$$

and H is the integral of H_λ over all wavelengths.

V. GENERAL REQUIREMENTS FOR MASSIVE STAR FORMATION

Larson and Starrfield (1971) discuss a number of momentum boundary conditions that must be satisfied for accretion to be maintained. In this section we reevaluate some of these conditions in terms of more recent understanding of interstellar grain properties.

a) Outer Boundary

Consider the conditions that must hold at the outer boundary of the flow. For inflow to occur the outward radiative acceleration per gram of gas must be less than the inward gravitational acceleration on that gas. This condition is conveniently written in terms of the ratio of the outward to inward accelerations, Γ,

$$\Gamma = \frac{k_H^{pr} L}{4\pi c G M(r_2)}\,, \tag{10}$$

where r_2 is the outer boundary of the flow. For infall, Γ must be less than unity. Note that Γ depends on the total luminosity to mass ratio, $L/M(r_2)$, at the outer boundary. This is not simply the luminosity-to-mass ratio of a ZAMS star because both L and $M(r_2)$ have additional contributions. The luminosity L, must include the accretion shock luminosity, L_{sh}; the mass $M(r_2)$ must include the mass contained within the shell, M_{shell} which can be comparable to the core mass. In this section let us simply assume that the shock luminosity has its maximum value, which corresponds to free fall of mass onto a hydrostatic core with mass M_* and radius R_*, at a mass infall rate of $\dot{M}$; i.e., $L_{sh} = GM_*\dot{M}/R_*$. Let us assume that the mass infall is radial and steady; therefore,

$$\dot{M} = 4\pi r^2 \rho\,|u| = \text{constant}\,, \tag{11}$$

where u is the gas velocity (u is negative for inflow). The mass contained within radius r is then

$$M(r) = 4\pi \int_{r_1}^{r} r^2 \rho dr + M_* = \dot{M}\int_{r_1}^{r} \frac{dr}{|u(r)|} + M_*\,, \tag{12}$$

where r_1 is the inner edge of the dust shell. To evaluate the gas velocity u, let us assume here that the inflow is in free fall:

$$u\frac{du}{dr} = -\frac{GM(r)}{r^2}. \quad (13)$$

Equations (11)–(13) can be solved for $M(r_2)$ by the numerical iteration discussed in Appendix A.

To estimate the flux mean opacity in equation (10) let us assume the radiation field is Planckian at a radiation temperature, T_{rad}, and derive the monochromatic opacity assuming the MRN mixture of grains. The MRN model is a reasonable mixture to assume for the initial precollapse cloud since it gives a good fit to the observed diffuse interstellar extinction law. The MRN mixture consists of bare graphite and silicate grains distributed in size as

$$n_i(a)da = A_i a^{-3.5} da ,$$

where A_i is a scale factor for each composition. Their grain size distribution runs from $a_- = 0.005$ μm to $a_+ = 0.25$ μm. The scale factors, A_i, have been determined empirically by DL from a fit to the observed extinction curve of Savage and Mathis (1979) and to the observed average galactic value of $N_H/E(B-V) = 5.8 \times 10^{21}$ of Bohlin, Savage, and Drake (1978). DL gives the values $\log A_C = -15.16$, $\log A_{Si} = -15.11$ (in units of $\mu m^{2.5}$ per hydrogen atom).

Now we have assembled all of the quantities required to evaluate Γ in equation (10) as a function of T_{rad}, $\dot{M}$, and M_* (and the associated L_* and R_* as derived from Maeder 1980). Let us consider a star with $M_* = 100\ M_\odot$ and $\dot{M} = 10^{-3}\ M_\odot$ yr^{-1}, for which $L_{sh} = 10^{5.34}\ L_\odot$ and $M_{shell} = 31\ M_\odot$. We find that the condition $\Gamma < 1$ at the outer boundary leads immediately to interesting new constraints.

Figure 2 shows Γ as a function of T_{rad} for our assumed MRN grain mixture. The radiation temperature at the outer boundary should have a value no larger than $\sim$2000 K since grains at the inner boundary will be sublimated at higher temperatures, and this sets an upper limit on the brightness temperature of the reradiated field. Note that Γ is much greater than unity for all plausible values of T_{rad} for the MRN mixture! This is already surprising. Infall of a massive protostellar cloud will not occur if the opacity is as large as that expected from the standard MRN mixture. If we insist that inflow occurs, then we must allow for modifications of the standard grain model.

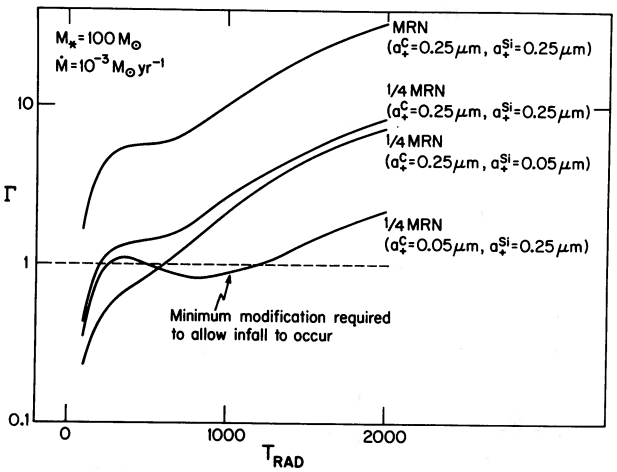

FIG. 2.—Ratio of outward radiative acceleration to inward gravitational acceleration, Γ, at the outer boundary of the dust shell vs. radiation temperature. For inflow to occur Γ must be less than 1. The shell mass ($=31\ M_\odot$) and shock luminosity ($=10^{5.14}\ L_\odot$) resulting from an accretion rate of $\dot{M} = 10^{-3}\ M_\odot$ yr^{-1} is accounted for in calculating Γ. Shown are curves using the standard MRN diffuse cloud grain mixture and three modifications to the standard grain model. Inflow is allowd over a wide range in T_{rad} for the grain model: $A_C = -15.76$, $A_{Si} = -15.71$ (one-fourth the overall scale factors determined by DL), $a_-^C = a_-^{Si} = 0.005$ μm, $a_+^C = 0.05$ μm, $a_+^{Si} = 0.25$ μm.

The modifications are shown in Figure 2. First, if we decrease the total grain-to-gas ratio by a factor of $\frac{1}{4}$, the value of Γ is similarly reduced but is still too large to allow infall. This reduction of the dust-to-gas ratio is considered plausible because it has been estimated that the dust abundance in the LMC (Koornneef 1982) and along some lines of sight in the Galaxy (Shull and Van Steenberg 1985) is down by a factor of $\frac{1}{4}$ relative to the standard Galactic value. Now let us consider the effects of modifying the sizes of the grains. Shown in Figure 2 is the effect of reducing the maximum silicate grain size from 0.25 to 0.05 μm. This reduces the value of Γ only slightly. Finally, we restore the full size scale for the silicates and reduce the maximum size for the graphite particles. This modification causes Γ to be less than unity for a rather broad range of T_{rad}. The modification of the graphite size limit brought on such a large change in Γ because in the MRN mixture, large graphite grains provides considerable opacity at visual and near-infrared wavelengths as can be seen in Figure 1*a* in WC1.

We conclude from this study that for inflow to occur, the total number of grains must be decreased by a factor of 4 or more from the standard Galactic number abundances, and the largest graphite grain size must be decreased. Clearly special grain conditions must exist for massive star formation to occur.

We show in Figure 3 the effects on Γ of varying the accretion rate. Shown are curves for the standard model, the three modifications of the standard model, plus a fifth curve showing the effects of an additional decrease in the total number abundance of grains. Table 1 lists a number of accretion rates and their corresponding L_{sh}, M_{shell}, L/M, r_2, and Γ. At low accretion rates, Γ is essentially independent of $\dot{M}$, this is because the shock luminosity and shell mass is small compared to the core luminosity and core mass. At higher $\dot{M}$, the additional increase

TABLE 1

ACCRETION ONTO 100 $M_\odot$ CORE

$\dot{M}$ ($M_\odot$ yr^{-1})	$\log L_{sh}$[a] ($L_\odot$)	M_{shell}[b] ($M_\odot$)	L/M (ergs s^{-1} g^{-1})	r_2[c] (cm)	Γ[d]
1×10^{-5}.....	3.34	4.0×10^{-3}	2.6×10^{4}	2.1×10^{16}	1.04
3×10^{-5}.....	3.82	3.4×10^{-2}	2.6×10^{4}	4.4×10^{16}	1.04
5×10^{-5}.....	4.04	9.7×10^{-2}	2.6×10^{4}	6.2×10^{16}	1.04
1×10^{-4}.....	4.34	3.9×10^{-1}	2.6×10^{4}	9.8×10^{16}	1.05
3×10^{-4}.....	4.82	3.5×10^{0}	2.6×10^{4}	2.0×10^{17}	1.05
5×10^{-4}.....	5.04	9.2×10^{0}	2.5×10^{4}	2.8×10^{17}	1.03
1×10^{-3}.....	5.34	3.1×10^{1}	2.3×10^{4}	4.2×10^{17}	0.92
3×10^{-3}.....	5.82	1.5×10^{2}	1.5×10^{4}	7.0×10^{17}	0.61
5×10^{-3}.....	6.04	2.8×10^{2}	1.2×10^{4}	8.5×10^{17}	0.49
1×10^{-2}.....	6.34	6.2×10^{2}	9.4×10^{3}	1.1×10^{18}	0.38
3×10^{-2}.....	6.82	2.0×10^{3}	7.3×10^{3}	1.6×10^{18}	0.30
5×10^{-2}.....	7.04	3.3×10^{3}	6.9×10^{3}	1.9×10^{18}	0.28
1×10^{-1}.....	7.34	6.7×10^{3}	6.6×10^{3}	2.4×10^{18}	0.27

[a] Assuming maximum shock luminosity $= GM_*\dot{M}/R_*$.
[b] Assuming free-fall collapse onto $M_* + M(r)$ (see Appendix A).
[c] The quantity r_2 is defined so that $\rho(r_2) = 10^{-19}$ g cm^{-3}.
[d] Evaluated at $T_{rad} = 1000$ K, for the grain model:
$a_+^C = 0.05$ μm, $a_+^{Si} = 0.25$ μm, $\log A_C = -15.76$, $\log A_{Si} = -15.71$.

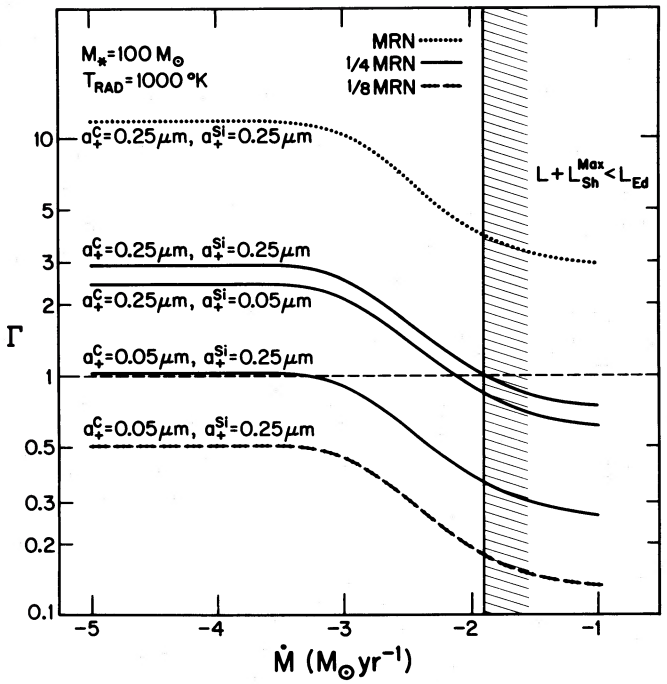

FIG. 3.—Ratio of outward radiative acceleration to inward gravitational acceleration, Γ, evaluated for T_{rad} = 1000 K at the outer boundary of the dust shell vs. mass accretion rate. Shown are curves for the MRN diffuse cloud grain model (*dotted*), grain models where the overall scale factors for both compositions are reduced by a factor of 4 (*solid*), and overall scale factors reduced by a factor of 8 (*dashed*). Accretion rates greater than $\dot{M} = 1.2 \times 10^{-2}$ produce a total luminosity greater than the core's Eddington luminosity.

in mass has a larger effect than the additional increase in luminosity so L/M and Γ decrease. We see that for all of the modified grain mixtures, Γ dips below 1 at extremely high $\dot{M}$, but the standard mixture is always greater than 1. Therefore, our conclusion, that infall of a MRN mixture cannot occur, remains valid.

At what core mass is inflow of a MRN mixture of grains allowed by the outer boundary condition? Figure 4 shows Γ versus T_{rad} for a number of core masses, where the standard MRN mixture is used to calculate all curves. We have used a logarithmic scale to plot T_{rad} in order to show the dependence of Γ on the cooler radiation temperatures. The adopted accretion rate for each core mass is the greater of 10^{-5} $M_\odot$ yr^{-1} or the inflow rate $\dot{M}_{min}$ (eq. [18]) calculated for the destruction radius, r_1, of a 0.25 μm graphite grain (see § V*b*). Figure 4 shows that infall onto a 60 $M_\odot$ core is allowed only if grains see a radiation field of color temperature much cooler than ~90 K. Considering the radiation field of the models presented later in this paper (T_{rad} ~ 150–200 K at the outer boundary) and the spectra shown in WC1, this simple outer boundary constraint is not satisfied for accretion onto a 60 $M_\odot$ core. We note that Larson and Starrfield adopted T_{rad} = 500 K to determine their limit and Kahn found T_{rad} = 900 K. We conclude from Figure 4 that core masses as low as 15–30 $M_\odot$ are probably required to have Γ < 1.

b) Inner Boundary

The visible and ultraviolet light from the core plus shock is absorbed in a thin "momentum deposition region" at the inner edge of the cocoon. For inflow to be maintained it is necessary that this outward momentum flux, $L/(4\pi r^2 c)$, be exceeded by the inward momentum flux or "ram pressure," ρu^2, of the infalling material. This condition can be written as a constraint on the mass inflow rate using the conservation of mass equation (11), yielding

$$\dot{M}_{min} > \frac{L}{u_1 c}, \tag{14}$$

where u_1 is evaluated just beyond the momentum deposition region. To provide an estimate of u_1 let us assume that a mass element is in free fall throughout the shell and ignore the gravitational acceleration of the mass element by the matter within the shell. Then $u_1 = (2GM_*/r_1)^{1/2}$, and we must estimate the inner radius of the shell r_1. We can estimate r_1 to be the radial distance at which the largest, most refractory grain ($a_+ = 0.05$ μm) is sublimated by heating from the central source. That is, we balance the absorption of UV and visible light from the central object with the reemission of infrared radiation from the grain when it is at its sublimation temperature, T_{sub} (which we here take to be ~1800 K); thus,

$$\frac{1}{(4\pi r_1)^2}\int Q^A(a,\lambda)L_\lambda\, d\lambda = \int Q^A(a,\lambda)B_\lambda(T_{sub})d\lambda\,. \tag{15}$$

If we, furthermore, assume that the central object radiates as a blackbody with an effective photospheric radius R_{ph} and an effective photospheric temperature T_{ph}, then

$$\int_0^\infty L_\lambda\, d\lambda = 4\pi R_{ph}^2 \int_0^\infty \pi B_\lambda(T_{ph})d\lambda$$
$$= L^* + GM_*\dot{M}/R_*. \tag{16}$$

As can be seen here, R_{ph} and T_{ph} depend on $\dot{M}$, and they can be determined by solving the equations (35)–(38) in WC1. Since the integral on the left side of equation (15) is weighted strongly

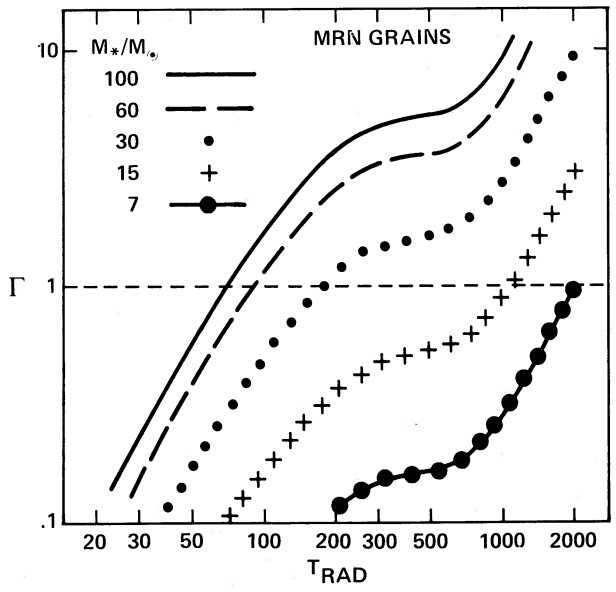

FIG. 4.—Ratio of outward radiative acceleration to inward gravitational acceleration, Γ, evaluated for a number of core masses vs. radiation temperature. For inflow to occur Γ must be less than 1. All curves are calculated using the MRN diffuse cloud grain model. The adopted accretion rates are 100 $M_\odot - \dot{M} = 3.7 \times 10^{-4}$ (eq. [18]); 60 $M_\odot - \dot{M} = 1.6 \times 10^{-4}$ (eq. [18]); 30 $M_\odot - \dot{M} = 3.4 \times 10^{-5}$ (eq. [18]); 15 $M_\odot - \dot{M} = 1.0 \times 10^{-5}$; 7 $M_\odot - \dot{M} = 1.0 \times 10^{-5}$.

to short wavelengths, we can assume the absorptive efficiency factor is near the geometrical optics limit, and to a fairly good approximation we can ignore the shock contribution in equation (16). With these simplifications, the equations give

$$r_1 = \left[\frac{Q^A(a)L^*}{(4\pi)^2}\Big/\int_0^\infty Q^A(a,\lambda)B_\lambda(T_{\rm sub})d\lambda\right]^{1/2}. \quad (17)$$

Detailed calculations as in WC1 show that $Q^A(0.05\ \mu\text{m}) \approx 1.35$ for all cores more massive than 15 $M_\odot$ and

$$\int Q^A(0.05\ \mu\text{m},\lambda)B_\lambda(1800\ \text{K})d\lambda = 1.24\times 10^7\ .$$

Eliminating u_1 from equation (14), we find

$$\dot{M}_{\rm min} = \frac{L^*}{c(2GM_*/r_1)^{1/2}}, \quad (18)$$

and this minimum mass inflow rate is shown as a function of core mass in Figure 5. The difference between the exact equation (14) and the approximate expression (18) is 8% for $M_* = 2000\ M_\odot$ and is 4% at 100 $M_\odot$.

Figure 5 also shows a number of less restrictive conditions on $\dot{M}$. In region A, the inflow rate is too small to keep the H II region compact. In this case the H II region expands into the dust shell where the gas pressure gradients are likely to halt the inflow of material. Below the limit marked "B" the inflow rate is too low to form a massive core in less than an evolutionary lifetime, i.e., $M_*/\dot{M} < \tau_{\rm ev}$. The limit noted as "C" corresponds to the case in which dynamic pressure is too small to drive the flow through the grain destruction radius discussed above. Region D is the allowed region for accretion to continue. Region E is an approximate upper limit on $\dot{M}$. In this region the core luminosity plus shock luminosity exceeds the core's Eddington luminosity. In this case, radiation pressure acting on electron scattering opacity will lift off the outer layers of the core. Since the contribution to the total luminosity from $L_{\rm sh}$ is proportional to $R_{\rm sh}^{-1}$, $L_{\rm sh}$ will decrease if the shock occurs before the flow reaches the surface of the core. Therefore we have plotted two upper limit curves in Figure 5. The first one uses the maximum possible shock luminosity $L^{\rm max}$, where $R_{\rm sh} = R_*$, and the second uses $L_{\rm sh} = 0.5L^{\rm max}$. Figure 5 gives us a roughly triangular zone in the ($\dot{M}$, M_*) plane for which accretion can occur. Note that the values of $\dot{M}$ are rather large ($\sim 10^{-3}$ yr^{-1}). Stahler, Shu, and Taam (1980) argue that a rough estimate of the protostellar accretion rate, $\dot{M}$, can be obtained from the relation

$$\dot{M} \sim (a_T^2 + v_{\rm A}^2 + v_t^2)^{3/2}/G\ , \quad (19)$$

where a_T is the isothermal sound speed in the initial protostellar cloud and $v_{\rm A}$, v_t are characteristic Alfvén and turbulent speeds. Any additional hydrostatic support of the initial cloud can be included by adding additional sources of signal speeds. The perhaps unexpected result that $\dot{M}$ increases with the initial hydrostatic support can be understood by considering the Jeans relation for gravitational instability,

$$M_{\rm J} = \left(\frac{\pi kT}{\mu m_{\rm H} G}\right)^{3/2}\frac{1}{\rho^{1/2}}; \quad (20)$$

as the gas temperature (or any other source of support) increases, the density must also increase if the cloud is to undergo gravitational collapse. Since the free-fall time is proportional to $\rho^{-1/2}$, the cloud will collapse on shorter time scales, thereby increasing the accretion rate.

It is convenient to define an equivalent temperature, $T_{\rm sup}$, representing the total hydrostatic support of the initial cloud:

$$T_{\rm sup} = \frac{\mu m_{\rm H}}{k}(G\dot{M})^{2/3}\ . \quad (21)$$

Shown along the right side of Figure 5 are a number of values of $T_{\rm sup}$ at their corresponding accretion rates. Note that the values of $T_{\rm sup}$ corresponding to our previously defined "allowed region" are rather high, $\sim 10^3$ K. This indicates that collapse of a massive star requires a very turbulent or warm region to produce the necessary accretion rates.

In estimating the velocity of r_1 we have not included the additional gravitational acceleration due to the mass contained within the shell. Using the calculated $\dot{M}_{\rm min}$ and an outer boundary r_2, at which $\rho(r_2) = 10^{-19}$ g cm^{-3} (Appendix A), we find that the mass contained within the shell never exceeds $\sim$40% of the core mass. This additional mass could increase the estimated velocities by at most a factor of 1.2, although at accretion rates greater than $\dot{M}_{\rm min}$ the additional mass can substantially increase the inflow velocities.

In this section we discussed limits on the accretion rate and new conditions on the initial grain model that must be satisfied in order for inflow to be maintained. Proper estimates of limits on $\dot{M}$ require us to account for the deceleration of the flow

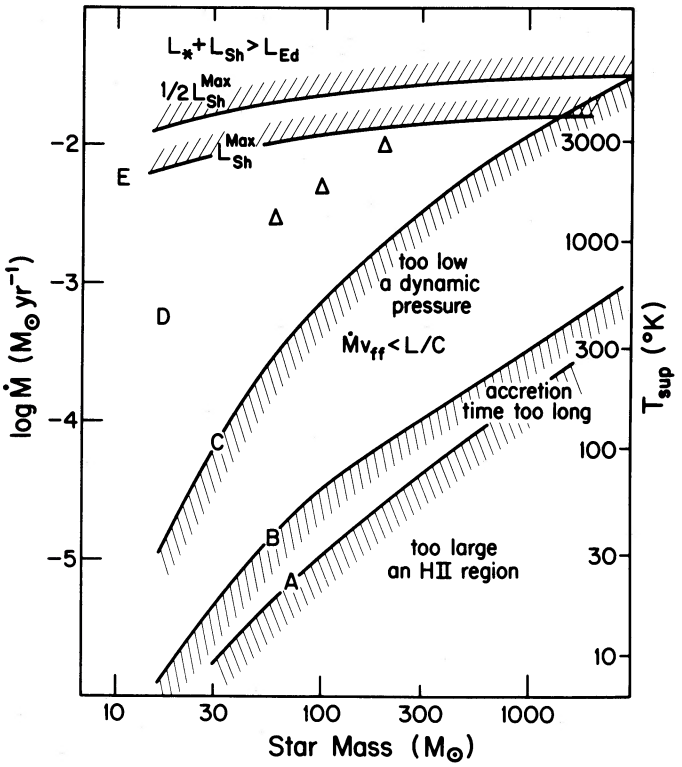

FIG. 5.—Region of accretion rate vs. core mass that allows inflow to occur (region D). Cores with accretion rates in region A have H II regions that expand beyond the dust destruction radius. Below the limit B the mass accretion time ($M_*/\dot{M}$) exceeds the core evolutionary lifetime. Inflows with accretion rates below C are halted by the stellar radiation field. Above the limit E the core plus shock luminosity exceeds the core's Eddington luminosity. Shown are curves for the maximum and one-half the maximum shock luminosity. The equivalent support temperature (eq. [21]) is shown on the right-hand side. The accretion rates of our numerical inflow models (§ V) are plotted (Δ).

between the shell boundaries due to radiation pressure acting on grains. This is because deceleration reduces the inflow speed as the matter approaches the shell's inner edge, and the resulting "ram pressure" will be less than that estimated from a free-fall velocity used in this section. This will raise the minimum required accretion rate above the minimum shown in Figure 5. The slower infall speeds may also demand that the grain number abundance be decreased to a value less than that estimated in Figure 2. To determine the actual gas inflow speed and obtain a better estimate to the accretion rate and grain abundance it is necessary to carry out numerical, hydrodynamic, and radiation transfer calculations.

VI. CALCULATION OF ACCRETION FLOWS

There have been a number of calculations of the earliest phase of cloud collapse, even accounting for three-dimensional flow (e.g., see Terebey, Shu, and Cassen 1984; Tohline 1980; reviews by Woodward 1978 and Bodenheimer 1983). The evolution of these models is generally halted when the assumption of isothermal collapse is no longer valid, although Boss (1984) has considered nonisothermal collapse in two-dimensional (Boss 1984) and in three-dimensional (Boss 1985) flow structure. These studies are mainly concerned with low-mass star formation prior to the creation of the hydrostatic core. Stahler, Shu, and Taam (1980) began with a low-mass hydrostatic core and evolved it through the main accretion phase. They developed a computational strategy whereby the major regions of the flow are described by separate radial equations. The results are smoothly joined between regions and stepped forward in time in a series of steady state solutions.

There are relatively few calculations of the main accretion phase of massive star formation. Appenzeller and Tscharnuter (1974), Yorke and Krügel (1977), and Yorke (1980) carried out time-dependent hydrodynamic calculations which trace the evolution of more massive clouds. Yorke and Krügel developed a model which treated grains and gas as two separate streams coupled by collisions. The separation of grains and gas is not considered to be appreciable in an accretion flow onto a low-mass star. In all of these calculations ice mantles are a major source of opacity in the outer regions of the flow. In fact, for the most massive cloud models, radiation pressure acting on icy grains was the dominant mechanism in halting the accretion.

For our calculations we assume that the accretion rate is constant over an infall time. Zinnecker and Tscharnuter (1984) have shown that for the case of a protostar embedded in a larger cloud, the rate of accretion is nearly constant over a large portion of the accretion phase. Under this assumption the radiation transfer and hydrodynamics can be written as steady state equations.

To account for grain destruction processes we treat grains and gas as separate streams. Grains of different sizes and compositions satisfy different momentum equations, and therefore the grains move relative to each other and relative to the gas stream. Rapid grain-gas relative velocities enhance ablation by chemical erosion, while high-speed grain-grain collisions lead to vaporization. We divide our size distribution into 15 sizes, creating 14 bins, for each of the two grain types. Therefore we account for the inflow of 30 grain streams plus one gas stream.

Ice mantles are not included on our grains. This eliminates the second or outer cocoon that appeared in the Yorke (1980), and Yorke and Krügel (1977) models which eventually led to the reversal of the accretion flow in the more massive Yorke and Krügel cores. The neglect of ice grains can be justified for the case of massive star formation for a number of reasons: (*a*) the process of massive star formation should occur in warm or turbulent regions, where $T_{\rm sup}$ in equation (21) is greater than 1000 K, or equivalently $v_{\rm turb} > 3$ km s^{-1}. Using equation (25) in Draine and Salpeter (1979*b*), we find that an H_2O ice mantle of 100 monolayers will sublimate in ~ 1 yr at grain temperatures of 150 K. If the grains are heated to these temperatures prior to cloud collapse, then ice mantles will be removed. (*b*) The discussion of conditions needed to allow inflow at the outer boundary in § V indicates that large grains have been destroyed as a precondition for massive star formation. Very massive stars do not necessarily form at all locations in a galaxy, and the required preconditioning may occur in localized zones by shocks (Seab and Shull 1983). The fragile icy mantles would be destroyed in shocks exceeding 30 km s^{-1} (Draine and Salpeter 1979*b*). (*c*) Our operating premise is that very massive stars do in fact exist. If icy mantles truly prevent their formation, we must neglect them as we do for the large graphite grains.

a) Grain Equation of Motion

The steady state equation of motion for a dust grain of composition i and size j is

$$w_{ij}\frac{dw_{ij}}{dr} = -\frac{GM(r)}{r^2} + \frac{F^{ij}_{\rm drag}}{m_{ij}} + \frac{\pi a_j^2 Q_{\rm H}^{\rm pr}(i,j)L}{4\pi r^2 m_{ij}}, \qquad (22)$$

where $M(r)$ is the total core plus shell mass that is contained within a sphere of radius r, $F^{ij}_{\rm drag}$ is the drag force exerted on grain (i, j) due to collisions with the surrounding gas, $Q_{\rm H}^{\rm pr}(i, j)$ is the flux mean radiation pressure efficiency, and m_{ij} is the mass of grain (i, j), $m_{ij} = (4/3)\pi a_j^3 \rho_i$. An expression for the drag force for neutral collisions is given by Draine and Salpeter (1979*a*):

$$F^{ij}_{\rm drag} = -2\pi a_j^2 k T_{\rm gas}\frac{\rho}{m_{\rm H}}\frac{8}{3\sqrt{\pi}} S\left(1+\frac{9\pi}{64}S^2\right)^{1/2}, \qquad (23)$$

where

$$S = \left[\frac{\mu m_{\rm H}}{2kT_{\rm gas}} v_d^2(i,j)\right]^{1/2}, \qquad (24)$$

$T_{\rm gas}$ is the gas temperature, μ is the average molecular weight of the surrounding gas, and $v_{\rm d}(i, j) = w_{ij} - u$ is the drift velocity between grain and gas streams. Following Krügel and Walmsley (1984), we estimate $T_{\rm gas}$ assuming it is determined by collisions with grains, giving

$$T_{\rm gas} = \frac{\sum_i \int_{a_-^i}^{a_+^i} n_i(a) T_a a^2 da}{\sum_i \int_{a_-^i}^{a_+^i} n_i(a) a^2 da}. \qquad (25)$$

b) Grain Continuity

The grain continuity equation must account for a number of interesting effects. (1) Grains of different sizes and compositions have different inflow speeds; therefore, we cannot use a single grain continuity equation to describe all grains. (2) Grain ablation processes decrease the size of grains but not the total number abundance of grains. At some point, however, grains become small enough to be considered "gas" rather than "grains." The abundance of grains smaller than this minimum size is considered to be zero, thereby removing grains from the stream. (3) Vaporization processes can be considered to decrease the abundance of grains at a particular grain size but not change the bin radii. (4) Grain destruction rates depend on grain temperature and velocity, and these are

different for each grain size. Even if we consider ablation alone, the shape of the grain size distribution will vary. Therefore, the grain continuity equation must conserve the total number of grains passing through a spherical shell per second but allow grains at a particular size to vary in abundance.

There are two major ways in which we can cast the continuity equation. First, we could follow the evolution of the grain distribution at a constant grain size, say a_1. In this case we would not keep track of any particular grain but only those of radius a_1. Grains initially at a_1 would be reduced in size and therefore decrease the number abundance at a_1, while larger grains are decreased in size which increase the number abundance at a_1. This would result in a series of rate equations to determine the abundances at a number of fixed grain sizes.

A simpler approach is to sample the grain distribution at a number of *initial* grain sizes and consider the evolution of these particular grains throughout the inflow. For the case of pure ablation processes the continuity equation is then decoupled from the number abundances of neighboring sizes, and we do not need to solve simultaneous equations (see Appendix B). We adopt this method and divide the grain distribution into 15 sizes between a_- and a_+, creating $j = 14$ grain "bins," of composition i. The continuity equation for each bin is simply

$$\frac{1}{r^2}\frac{d}{dr}(r^2 w_{ij} N_{ij}) = -R_{ij} N_{ij}\,, \quad i = 1, 2, j = 1, \ldots, 14\,, \tag{26}$$

where w_{ij} is some average velocity for grains in the bin, R_{ij} is the average fraction of grains destroyed in bin N_{ij} due to vaporization processes, and N_{ij} is the number density of grains in bin ij:

$$N_{ij} = \int_{a_j^i(r)}^{a_{j+1}^i(r)} n_i(a)da\,\frac{X\rho}{m_{\rm H}}\,. \tag{27}$$

The bin edges $a_j(r)$, $a_{j+1}(r)$ vary because of grain ablation processes.

b) Gas Equation of Motion and Continuity

The steady state equation of motion for the gas flow is

$$u\frac{du}{dr} = -\frac{GM(r)}{r^2} - \frac{1}{\rho}\frac{dP}{dr} + \frac{F_{\rm drag}}{\rho}\,, \tag{28}$$

where it is assumed that radiation pressure on the gas is negligible. The drag force is a result of the ensemble of grains colliding with gas particles

$$\frac{F_{\rm drag}}{\rho} = -\sum_i \int_{a_-^i}^{a_+^i} n_i(a, r) F_{\rm drag}^{ij}\, da\,\frac{X}{m_{\rm H}}\,. \tag{29}$$

The gas continuity equation has already been defined by equation (11). Note that equation (22) represents 30 differential equations (two compositions × 15 grain sizes) for the grain velocities, and the gas flow velocity (eq. [28]) is a function of all 30 grain velocities. This system can be greatly simplified following the arguments of Gilman (1972) that grains travel at a local terminal velocity. The outward radiative force on grains at every radial distance is balanced by the inward gravitational plus drag forces, so the gas and grains are momentum coupled, and all of the radiative momentum absorbed by the grains is transferred to the gas. Under these conditions the acceleration for the grains in equation (22) is equal to zero. Multiplying equation (22) by m_{ij} and then operating on the equation with

$$\sum_i \int_{a_-^i}^{a_+^i} n_i(a', r)\frac{X}{m_{\rm H}} \ldots da'\,, \tag{30}$$

and adding the results to equation (28), we find the gas equation of motion:

$$u\frac{du}{dr} = -\frac{GM(r)}{r^2}\left[1 + \sum_i \int_{a_-^i}^{a_+^i} n_i(a, r)\frac{4}{3}\pi a^3 \rho_i\, da\,\frac{X}{m_{\rm H}}\right] - \frac{1}{\rho}\frac{dP}{dr} + \frac{k_{\rm H}^{\rm pr} L}{4\pi r^2 c}\,, \tag{31}$$

where $k_{\rm H}^{\rm pr}$ is the flux mean radiation pressure coefficient (eq. [8]). The second term within brackets is the grain-to-gas mass ratio. Note that the drag force of the collection of grains acting on the gas is equal and opposite to the drag force of gas acting on the collection of grains. As a result, the drag cancels, and the gas equation of motion does not depend on the grain velocities. The evaluation of $k_{\rm H}^{\rm pr}$ in equation (31) requires a knowledge of the frequency-dependent radiation field as well as the grain number and size distribution.

For the dynamics of the flow, we have ignored gas pressure gradients and focused attention on the effects of drag forces and radiation pressure gradients. The gas temperatures are very low, and most of the flow is supersonic. The gradient of the gas pressure might be significant at the shell's inner edge, and then only if the gas flow is decelerated to sonic speeds. The dynamical effects of the finite temperature of the gas at the inner boundary perhaps warrants further investigation. Gas pressure gradients are usually ignored in the case of dust driven outflows of cool star winds (Kwok 1975; Cassinelli 1979; Castor 1981).

With the assumption that grains travel at their local terminal velocity equations (22), (23), and (24) can be solved for the grain drift velocities:

$$v_{d_{ij}}^2 = -\frac{64kT}{9\pi\mu m_{\rm H}} + \left[\left(\frac{64kT}{9\pi\mu m_{\rm H}}\right)^2 + \frac{16a_j^2\rho_i^2}{9\rho^2}\left\{\frac{GM(r)}{r^2}\left[1 - \frac{\pi a^2 Q_{\rm H}^{\rm pr} L}{m_{ij} 4\pi c GM(r)}\right]\right\}^2\right]^{1/2}\,, \tag{32}$$

and the grain velocities can be obtained from

$$w_{ij} = u + v_{d_{ij}}\,. \tag{33}$$

d) Destruction Processes

As the grains fall inward, the initial size distribution will be modified by ablation and vaporization processes. We calculate the ablation processes of sublimation for both graphite and silicate grains and erosion by surface chemical reactions on graphite grains. We also consider vaporization by grain-grain collisions for both graphite and silicate grains.

i) Sublimation

The rate of sublimation can be estimated from the vapor pressure of the grain material (Palmer and Shelef 1968; Lamy 1974). The rate at which a grain of composition i and radius a is decreased in size as it falls inward is given by

$$w_i(a)\left.\frac{da^i}{dr}\right|_{\rm sub} = \frac{P_{\rm vap}(T_a^i)}{\rho_i}\left(\frac{\mu_i m_{\rm H}}{2\pi k T_a^i}\right)^{1/2}\,, \tag{34}$$

where T_a^i is the grain temperature as a function of both size and composition, $P_{\rm vap}(T_a^i)$ is the vapor pressure of the grain material at temperature T_a^i, and μ_i is the molecular weight of the evaporated molecules. We have assumed in writing equation (34) that the accommodation coefficients in the equation of Lamy (1974) are unity and the temperature of the vapor is

TABLE 2

GRAIN PROPERTIES

Parameter	Graphite	Silicate
m_i (amu)[a]	12.0	169.1
ρ (g cm^{-3})[b]	2.26	3.30
$E_{\rm bind}$ (eV)[c]	11.03	6.75
α[d]	16.346	14.570
β[d]	40673	26335

[a] Molecular weight of grain material assuming silicate composition is $Mg_{1.1}Fe_{0.9}SiO_4$; Draine and Lee 1984.

[b] Density of grain material; Draine and Lee 1984.

[c] Binding energy; Shull 1978.

[d] Vapor pressure, log P(dyne cm^{-2}) $= \alpha - \beta/T$; Lamy 1974, Leider, Krikorian, and Young 1973.

the same as the grain temperatures. For graphites we use the vapor pressure data of Leider, Krikorian, and Young (1973). For silicates we assume the vapor pressure of quartz given by Lamy (1974). Since astronomical grains are almost certainly not crystalline in structure, we are underestimating the vapor pressure or overestimating the grain temperatures over which sublimation occurs. Table 2 lists grain parameters used in our destruction equations.

ii) *Graphite Grain Surface Reactions*

Barlow and Silk (1977) proposed that hydrogen reacting with C on graphite grain surfaces can erode interstellar graphite grains. Through a series of interaction steps, four hydrogen atoms combine with C to form a CH_4 molecule. The molecule then evaporates from the grain surface, thereby removing a lattice C atom. The reaction rates determined by Draine (1979) are used to estimate the rate at which the grain radius is decreased:

$$w \left.\frac{da}{dr}\right|_{\rm sur} = \frac{n({\rm H\ I})Y(T_a)\mu_{\rm C} m_{\rm H} v_{\rm rel}}{4}, \quad (35)$$

where n(H I) is the number density of atomic hydrogen, $Y(T_a)$ is the yield of carbon atoms removed per incident hydrogen atom taken from (Draine 1979), $\mu_{\rm C}$ is the molecular weight of carbon, and $v_{\rm rel}$ is the relative velocity between grain and gas streams.

The total rate of grain ablation is thus the sum of the rate of destruction by sublimation and surface reactions:

$$w\frac{da}{dr} = w\left.\frac{da}{dr}\right|_{\rm sublimation} + w\left.\frac{da}{dr}\right|_{\rm surface\ reactions}. \quad (36)$$

To calculate these destruction rates we need to know the grain temperatures at all radial distances through the accretion flow and this is derived as discussed in WC1.

iii) *Vaporization*

Seab and Shull (1983) calculate grain vaporization rates resulting from grain-grain collisions in interstellar shocks. They account for grains of different sizes and compositions. The grain collisions are a result of the gyromotion of grains moving in a magnetic field. In our calculations we only consider the "head on" collisions of grains due to different relative inflow velocities.

The number of grains of composition i vaporized as a result of grain-grain collisions in the range a to $a + da$ per cm^3 per second is

$$n_i(a)\frac{X}{m_{\rm H}}\rho R(a) = n_i(a)\left(\frac{X\rho}{m_{\rm H}}\right)^2 \times \sum_l \int_{a-l}^{a+l} n(a')f_T(v_{\rm rel})\sigma(a, a')\,|\,w_l(a') - w_i(a)\,|\,da', \quad (37)$$

where $R(a)$ is the fraction of grains of radius a destroyed per second, l is summed over all compositions, $\sigma(a, a')$ is the collision cross section for grains of sizes a, a', and $f_T(v_{\rm rel})$ equals 0 or 1, depending on whether the relative velocity of colliding components is larger than the threshold velocity for vaporization. Following Seab and Shull, we account for two threshold velocities because in collisions between grains of unequal masses the lighter grain is assumed to vaporize first, while the more massive one is vaporized only if sufficient energy is left over. If m is the mass of the lighter grain moving at a speed w, M is the mass of the more massive one with speed W, and m_r is their reduced mass [$=mM/(m + M)$], then the lighter one vaporizes if the relative kinetic energy, $\frac{1}{2}m_r(w - W)^2$, exceeds the binding energy of the lighter particle ($mE_{\rm bind}/m_i$, in Seab and Shull, where m_i is the mass of the molecules in grain m). The more massive one vaporizes, if the relative kinetic energy exceeds the sum of the binding energies. As we shall see, the vaporization process is found to be a relatively minor destruction process for our models.

e) The Numerical Method

Given a core mass M_*, an accretion rate $\dot{M}$, and an initial grain model, such as a depleted MRN mixture, the calculations provide the gas density and velocity distributions as a function of radial position in the shell as well as the spatial distributions of velocity, temperature, and grain sizes at the bin edges, and the number densities $N_{ij}(r)$ at the centers of each of the 28 grain bins. These quantities are derived using basically a two-step interaction. One step provides the structural variables such as density and grain sizes, and the other step provides the internal radiation field and grain temperatures. The calculations need a zero-order model. This is found by specifying the outer density $\rho(r_2)$, and by solving equations (A1)–(A7) to provide a starting run of $\rho(r)$ and the value of the outer boundary r_2. The number abundances of the grains per H atom is initially taken to be constant as a function of radius, and the temperatures are assumed to fall as $T(r) = 2000\ {\rm K}(r/r_1)^{-0.4}$, where r_1 is the inner radius of the shell. The value of the inner radius is initially taken to be the position where a graphite grain of size $a = 0.05\ \mu$m has an equilibrium temperature of 2000 K, when it is exposed to spatially diluted stellar radiation. Then we can begin the two-step model calculation.

1. Given the current estimate of the gas and grain density distributions and grain temperature distributions, the radiation field in the shell is computed. The radiative equilibrium temperature distributions for grains at the edge of each bin was found by using the transfer method and temperature correction procedure of our previous paper (WC1). 2. The equations of motion (eqs. [31]–[33]), continuity (eqs. [11] and [26]), and grain destruction rates (eqs. [34]–[37]) are solved simultaneously as an initial boundary value problem by integrating inward from the outer boundary of the shell. At the boundary, r_2, the gas and grains are assumed to have the velocity of free fall from infinity, with the density $\rho(r_2)$. The inward solution uses the radiation field derived in step 1 in finding the radiative

acceleration on the grains, and it uses the temperatures in computing the sublimation destruction rates. The grain continuity equation requires special consideration. If vaporization is negligible, the grain continuity equation is simply $N_{ij} w_{ij} r^2 = C_{ij}$ where C_{ij} is a constant evaluated at the outer boundary. However, if vaporization occurs, equation (26) must be solved. This is done by first estimating $N_{ij}(r)$ ignoring vaporization, substituting the result into the right-hand side of equation (26), then solving the equation for a new estimate of N_{ij}. This procedure converges in two or three iterations.

The inward integration proceeds until all of the grains have been destroyed, which in our case means that they have reached a size smaller than 0.005 μm. The radial distance at which the last grains are destroyed is the inner boundary of our shell (we do not follow the flow inward from there, but assume the cool gas falls at the free-fall rate toward the star). If the structure through the shell has changed significantly from the previous iteration, steps 1 and 2 are repeated.

The structure near the inner boundary is the slowest to converge. This is because there is a steep temperature and velocity gradient as the inner boundary is approached. The inner boundary region is where the stellar ultraviolet radiation is absorbed and converted to infrared radiation. Dynamically it is where the momentum of the ultraviolet light is deposited, thereby reducing the inflow speed. To account for the steep temperature gradient and redistribution of radiation, the transfer solution requires a large number of radial grid points. We typically use 150 grid points altogether, with 50 near the inner boundary. The calculations are made somewhat complicated by the tendency for the inner boundary to drift. That is, in solving the structure equation the radius at which the last grain is destroyed can change from one iteration to the next. For example, if the inner radius moves outward, on the next iteration the grains at the new inner boundary are exposed to direct star light, while on the previous iteration that light had been partially attenuated by the grains lying closer to the star. To accelerate the convergence of the inner boundary, we find it useful to repeat step 1 at several values of the inner radius and choose the value for which the boundary drift is small. Then convergence of the inner boundary location and temperature structure can be found in a few iterations. The velocity structure also poses a problem near the inner boundary. This is mostly because of the nature of the problem as we have chosen to pose it. We want to find conditions that will just barely allow the inflow to occur. This is one in which the inflow speed almost decelerates to zero near the inner boundary. Since the gradient in speed is steep, with the inflow speed typically dropping from say 15 km s^{-1} at $1.01r_1$ to $\sim$1 km s^{-1} at $1.0r_1$, a slight change in dust properties near the inner boundary can make an amplified change in the value of the speed at r_1. The models are well converged in any case. Ignoring the very innermost point, the velocity, gas density, grain densities, and temperatures are converged to less than 1%. At the inner boundary point, the velocity $u(r_1)$ is converged to 3% for the 60 $M_\odot$ model and 10% for the 100 $M_\odot$ model and was bracketed to 2 ± 1 km s^{-1} in the 200 $M_\odot$ case.

Another problem concerning the inner boundary becomes important for the highest mass cores. If surface reactions completely dominate the grain destruction, we find the inner boundary moves outward with each iteration. Eventually a situation is reached in which the gas flow has not enough speed or "ram pressure" to allow it to overcome the outward radiative momentum that is deposited in the grain destruction region. As long as the surface reaction rate is not too high, a solution can be found. For the case of our 200 $M_\odot$ core we avoided this problem by decreasing the $n(\mathrm{H\ I})/n(\mathrm{H_2})$ abundance ratio and thereby reducing the effects of surface reactions.

Of course, not all of the models attempted resulted in inflow. If the inward flow was halted *before* all of the grains were destroyed, we restarted the model with different parameters. Our approach does not allow for circulation, but requires a steady flow in the inward direction. After finding an unsuccessful model, we would adjust, say, the dust-to-gas ratio or increase the mass inflow rates and try again. We feel the procedure used has led to useful insight into the conditions required for accretion toward very massive protostars. It shows, in particular, that the semianalytical conditions that have been discussed in § V require some modifications when more realistic radiative transfer and dust destruction mechanisms are accounted for.

VII. RESULTS AND DISCUSSION

Let us discuss in some detail the results for the 100 $M_\odot$ core. The model is computed using an accretion rate of $\dot{M} = 5 \times 10^{-3}\ M_\odot\ \mathrm{yr}^{-1}$. This inflow produces a maximum shock luminosity of $\sim 10^{6.04}\ L_\odot$ and a shell mass of 299 $M_\odot$. At the outer boundary a grain size distribution is assumed having minimum and maximum sizes $a_-^{\mathrm{C}} = 0.005$ μm, $a_+^{\mathrm{C}} = 0.02$ μm and $a_-^{\mathrm{Si}} = 0.005$ μm, $a_+^{\mathrm{Si}} = 0.2$ μm for the graphite and silicate grains, respectively. The overall scale factors are reduced by a factor of 8 from the standard Galactic values, yielding $\log A_{\mathrm{C}} = -16.06$, $\log A_{\mathrm{Si}} = -16.01$ (per H atom per $\mu\mathrm{m}^{2.5}$); see Table 3 for a complete list of model parameters). Note that, as expected, these maximum grain sizes and number abundances are smaller than those estimated in Figure 2. Also, the radiation pressure gradient has decelerated the flow and further constrained the grain distribution and mass accretion rate that will allow infall.

a) Velocity Structure

Figure 6*a* shows the run of grain and gas velocities as a function of distance from the central star. Relative to the free-fall velocity distribution, we see that the radiative pressure gradients have reduced the inflow speed throughout the shell even in the outer regions where the radiation field is peaked in the infrared and $k_{\mathrm{H}}^{\mathrm{pr}}$ is small. Figure 6*b* shows an expanded view of the rapid deceleration region near the inner edge of the shell. This rapid deceleration region is the UV momentum deposition region discussed in § V. The change in acceleration simply reflects the increase in opacity and hence in $k_{\mathrm{H}}^{\mathrm{pr}}$ for a radiation field peaking at shorter wavelengths.

In Figure 6*b*, we see that the drift velocities are higher for the larger grains. Factors affecting this drift speed can be isolated by examining equation (22). Consider the region near the inner edge of the shell. Here the dominant accelerations are the outward radiative pressure gradient and the inward drag acceleration. If we ignore the gravitational acceleration, consider the case where the drift speed is large compared to the thermal gas speed, and eliminate ρ using the gas continuity equation, then equation (22) yields

$$v_d = w - u = \left(\frac{Q_{\mathrm{H}}^{\mathrm{pr}} L |u|}{\dot{M} c} \right)^{1/2} . \tag{38}$$

The grain geometrical cross section, πa^2, is seen to have cancelled out, leaving $Q_{\mathrm{H}}^{\mathrm{pr}}$ as the only grain-dependent term.

TABLE 3

MODEL RESULTS

PARAMETER	STAR MASS M_* ($M_\odot$) 60	100	200	NOTES
I. Envelope Structure:				
Mass inflow rate $\dot{M}$ ($M_\odot$ yr^{-1})	3×10^{-3}	5×10^{-3}	1×10^{-2}	
Inner radius r_1 (cm)	3.86×10^{15}	4.48×10^{15}	9.81×10^{15}	
Outer radius r_2 (cm)	7.18×10^{17}	8.51×10^{17}	1.07×10^{18}	
Density at inner radius $\rho(r_1)$ (g cm^{-3})	1.40×10^{-15}	5.76×10^{-15}	2.69×10^{-15}	
Mass of shell $M_{\rm shell}$ ($M_\odot$)	177	299	587	
Total luminosity $L^* + L_{\rm sh}$ ($L_\odot$)	1.05×10^6	2.43×10^6	6.78×10^6	
Shock luminosity $L_{\rm sh}$ ($L_\odot$)	5.19×10^5	1.10×10^6	2.99×10^6	
$L_{\rm tot}/r_1^2$ (ergs s^{-1} cm^{-2})	2.69×10^8	4.88×10^8	2.68×10^8	
Velocity at r_1:u_1 (km s^{-1})	7.21	1.45	1.93	
Maximum inflow velocity $u_{\rm max}$ (km s^{-1})	13.4	11.9	16.8	
Envelope crossing time (yr)	5.89×10^4	5.32×10^4	5.86×10^4	
II. Grain and Gas Properties:				
n(H I)/n(H_2)	5×10^{-5}	5×10^{-5}	2×10^{-5}	1
Graphite scale factor relative to Galactic A_C/A_C°	1/8	1/8	1/13	2
Silicate scale factor relative to Galactic $A_{\rm Si}/A_{\rm Si}^\circ$	1/8	1/8	1/13	2
Maximum graphite grain radius $a_+^{\rm C}$ (μm)	0.02	0.02	0.015	
Maximum silicate grain radius $a_+^{\rm Si}$ (μm)	0.20	0.20	0.10	
Dominant destruction process	Sublimation	Surface reaction plus sublimation		
Ratio of sublimation rate to chemical reaction rate $\chi_{\rm sub}$	31	0.61	0.57	3
Ratio of drift to gas speed $\lvert v_d/u \rvert$	0.43	0.85	0.99	3
Graphite sublimation rate $da/dt\lvert_{\rm sub}$ (μm yr^{-1})	1.0×10^{-2}	4.7×10^{-4}	5.6×10^{-5}	3
Graphite surface reaction rate $da/dt\lvert_{\rm sur}$ (μm yr^{-1})	3.3×10^{-4}	7.8×10^{-4}	9.8×10^{-5}	3
Silicate sublimation rate $da/dt\lvert_{\rm sub}$ (μm yr^{-1})	2.4×10^{-2}	4.2×10^{-2}	1.4×10^{-1}	3
Maximum mass fraction of grains vaporized/grain size at bin center $/a$ (% μm^{-1})	2/0.10	3/0.10	1.5/0.023	
Maximum graphite drift speed/grain size v_d/a (km s^{-1} μm^{-1})	7.7/0.019	6.1/0.018	8.6/0.014	
Maximum silicate drift speed/grain size v_d/a (km s^{-1} μm^{-1})	6.7/0.017	6.6/0.180	7.9/0.069	
Gas temperature $T_{\rm gas}$ (K)	1680	1600	1540	3
Gas temperature at r_1 $T_{\rm gas}(r_1)$ (K)	1680	1740	1690	

NOTES.—(1) Leung, Herbst, and Huebner 1984; Iglesias 1977. (2) Using Galactic scale factors from Draine and Lee 1984, $\log A_C^\circ = -15.16$, $\log A_{\rm Si}^\circ = -15.11$. (3) Evaluated at the radial distance at which 90%–95% of the mass of the largest grain has been removed.

Therefore large grains have a greater drift speed only because their scattering and absorption efficiencies are greater than those of the smaller grains and not because of their greater mass or area. The drift speed is proportional to $u/\dot{M}$, so, as the gas velocity, u, decreases at the shell's inner edge, the gas density increases, causing the drift to diminish. This increase in gas density keeps grains flowing inward even though the gas velocity itself is slowing down. The additional thermal terms in equation (22) modify these results only slightly, in the sense that an increase in temperature at the inner edge reduces the drift velocities.

The use of a flux mean opacity rather than a Rosseland mean opacity that is sometimes used in inflow calculations has an important effect on the velocity distribution. This is illustrated in Figure 7. The solution using a Rosseland mean predicts only a small deceleration of the flow near the inner edge. This is because it does not account for the strong peaking of the radiation field toward the ultraviolet wavelengths with its attendant increase in the radiative acceleration on each grain. Other differences from calculations that use Rosseland opacities have been discussed in WC1.

b) Grain Destruction

Figure 6*b* shows that grains of different sizes and compositions are destroyed at different distances from the central star. The silicates tend to be destroyed farther out than do graphites, and small grains are destroyed before larger grains. We had expected that the range in distances over which the various grains are destroyed would be larger because, as discussed in WC1, there can be significantly different grain temperatures at a given position and there can be significant differences in grain velocities. However, our calculations yield a rather steep temperature distribution near the inner boundary of the shell, and the gradient in drift velocities is also rather large at that location. The net effect is that for our 100 $M_\odot$ model the large and small graphite grains are destroyed where the temperature is $\sim$1700 K.

Figure 8 shows the relative importance of each of the destruction processes. The differences in grain temperatures explain the differences in sublimation rates from large to small grains of the same composition. The rise in temperature of all grains toward the inner boundary explains the increase in sublimation rates there. For graphite we have also considered the ablation brought on by surface chemical reactions. Figure 8 shows that the rate for this process is 1.6 times that for sublimation for the large grain and 3.6 times the sublimation rate for the small grains.

Vaporization by grain-grain collisions for the 100 $M_\odot$ model is minor, even though the relative velocities exceed the vaporization threshold for collisions between a moderate-sized silicate grain and larger graphite or silicate grains. The vaporization is no more than $\sim$3% of the silicate mass. No vaporization occurs for the grains of the largest and smallest sizes. There are no collisions energetic enough to destroy both large

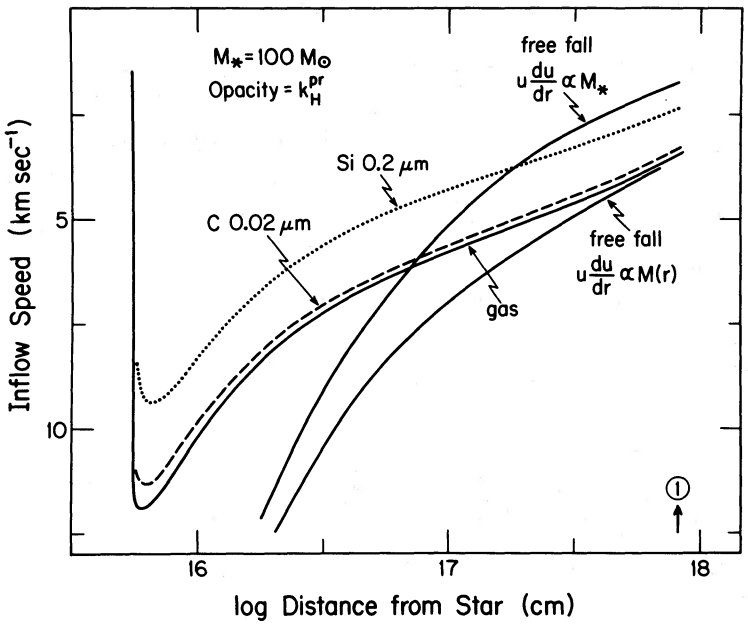

FIG. 6a

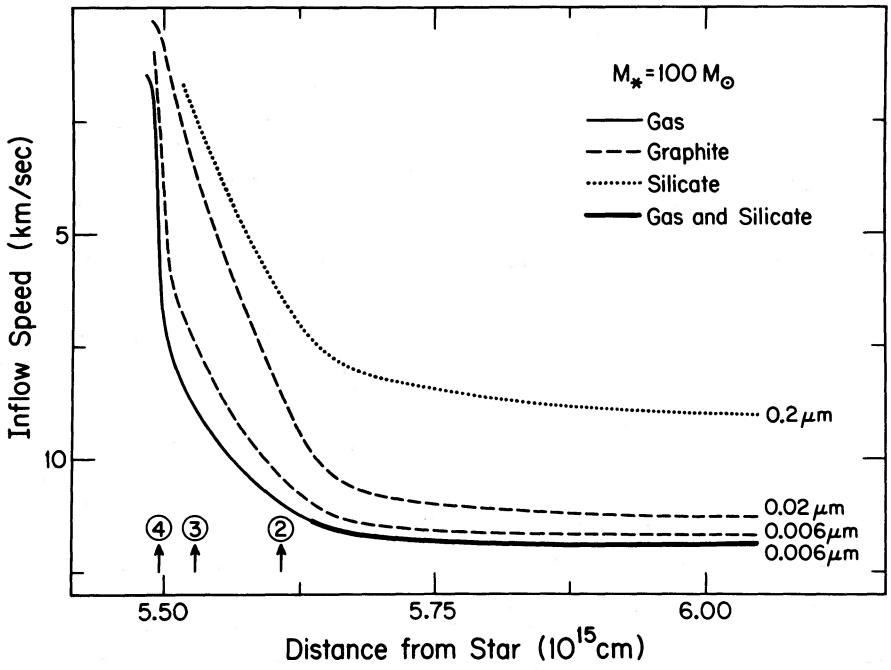

FIG. 6b

FIG. 6.—(*a*) Inflow speed onto a 100 $M_\odot$ core using flux mean radiation pressure opacities. Speeds are plotted for the full range in radial distance from inner to outer dust shell boundaries. Curves are shown for graphite grains of initial size 0.02 μm (*dashed*), silicate grains of initial size 0.2 μm (*dotted*), and gas (*solid*). Also shown are free-fall velocity curves accounting for the total (core plus shell) mass, $M(r)$, and the core mass alone, M_*. (*b*) Expanded view of (*a*) near the inner shell boundary. Curves are shown for graphite grains of initial sizes 0.02 and 0.006 μm (*dashed*), and silicate grains of initial sizes 0.2 μm (*dotted*) and 0.006 μm (*heavy solid*), and gas (*solid*). Curves end where grains are destroyed. Circled numbers along the abscissa in Figs. 5*a* and 5*b* refer to radial distances at which the grain size distribution is plotted in Fig. 9.

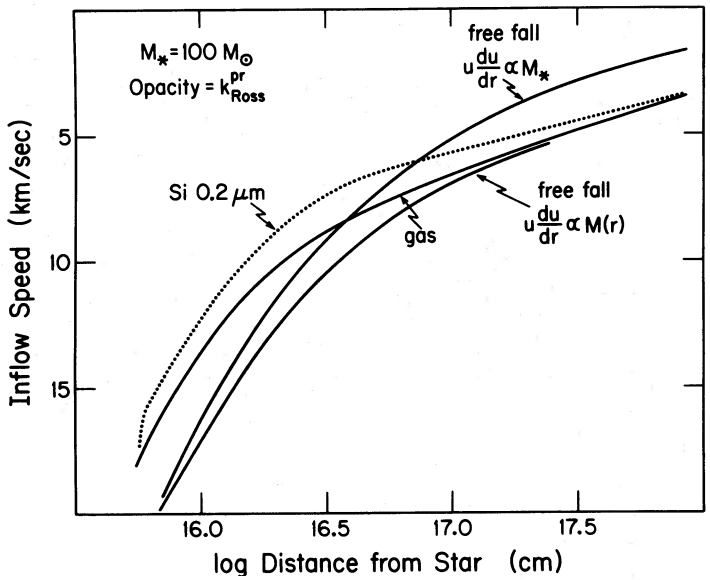

FIG. 7.—Inflow speeds onto a 100 $M_\odot$ core using Rosseland mean radiation pressure opacities. Curves are shown for silicate grains of initial size 0.2 μm (*dotted*) and gas (*solid*). Also plotted are free-fall velocity curves accounting for the total (core plus shell), mass, $M(r)$, and the core mass alone, M_*. Inflow speed for graphite grains are indistinguishable from the gas speeds when plotted on this scale.

and small colliding components and vaporization of graphite grains is negligible. These conclusions could be somewhat different for flows with smaller values of $\dot{M}$, because there would be a broader deceleration zone and higher relative grain velocities. In hindsight we see that we could have ignored vaporization and considered only the dominant mechanisms of sublimation and ablation by surface chemical reactions.

c) *Additional Grain Constraints*

We found that to allow infall in our numerical calculations we had to further constrain the grain models predicted in § V. We consider two causes for these modifications. The first involves the assumption of steady state inflow, and the second is a result of the radiative deceleration of gas at the shell's inner edge.

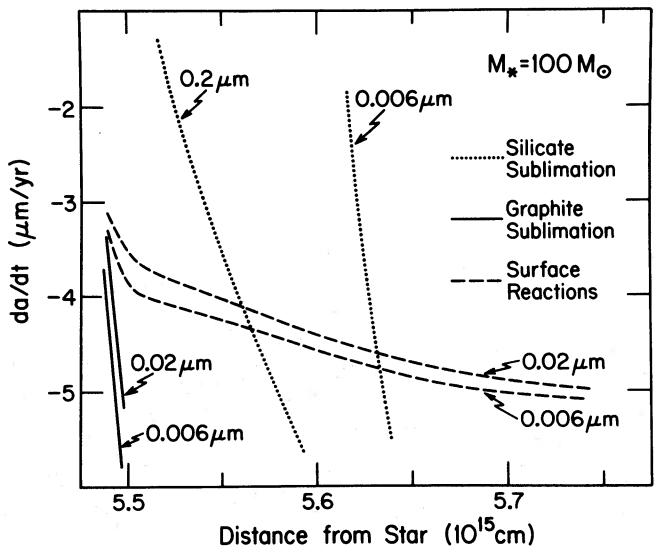

FIG. 8.—Grain destruction rates vs. radial distance for our 100 $M_\odot$ model. Plotted are graphite sublimation rates (*solid*) and surface reaction rates (*dashed*) for grains of initial sizes 0.02 and 0.006 μm. Sublimation rates for silicate grains (*dotted*) are plotted for grains of initial sizes 0.2 and 0.006 μm.

The assumption that grains travel at their local terminal velocity forces grains to have a unique drift velocity at every radial distance. If the required drift velocity were to exceed the gas flow velocity then grains would travel outward relative to the central star. Also, grains would be stopped in the flow if the drift velocity equals the gas velocity. At such a point the grain abundance could perhaps be determined by the length of time that grains have been collecting or piling up. However, these possibilities for grain velocity reversal and piling up violate our assumption of steady state flow. Since we are unwilling in this paper to eliminate the steady flow assumption, we must only consider cases for which grains are never stationary with respect to the central star. Since large grains have the largest drift velocity (see eq. [38]) we must decrease the largest grain sizes to ensure that all grains flow inward.

The second reason for additional grain modifications is the radiative deceleration of the flow which was not accounted for in § V. Our estimates for the grain abundances were there calculated by momentum considerations at the outer boundary. To find the velocity of gas at the inner boundary, it is necessary to carry out the full radiation transfer–hydrodynamic calculations. Using our estimate of § V for the grain abundances we find the gas flow is brought to a halt before the grains are destroyed. It is necessary, therefore, to reduce further the grain abundances to allow infall to continue. We did not examine the full range of abundances between one-fourth and one-eighth of the Galactic value, but simply chose to use this abundance. We do not consider one-eighth to be a firm limiting value, but consider that a substantial reduction in dust abundances is necessary for the very massive stars to form.

d) *Evolution of the Grain Size Distribution*

Figure 9 shows the grain size distributions for the graphites and silicates at a number of locations in the flow. These positions are indicated in Figures 6*a* and 6*b*. At the outer boundary

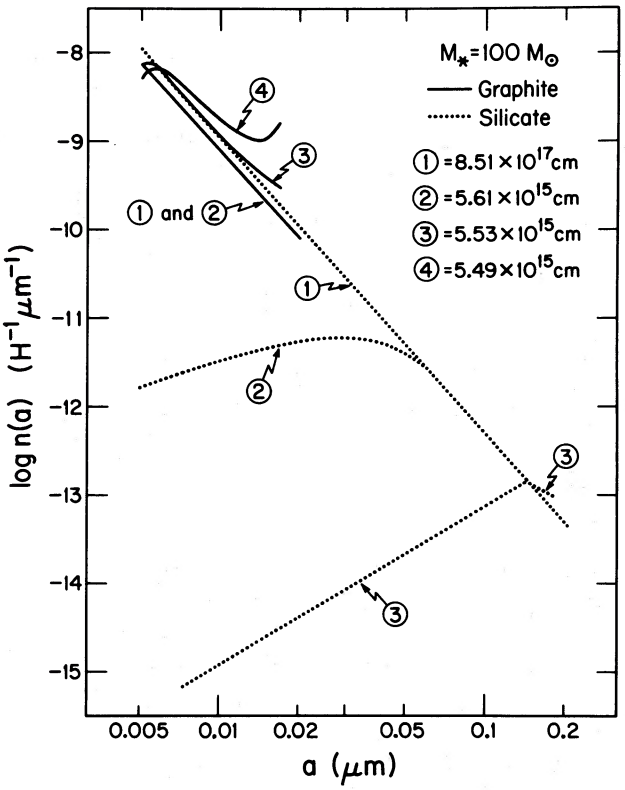

FIG. 9.—Evolution of the grain size distribution for our 100 $M_\odot$ model. Circled numbers refer to the radial distances from which the distributions are plotted (see Figs. 6*a* and 6*b*). Curves are shown for graphite (*solid*) and silicate (*dotted*) grain size distributions at four locations in the inflow. Silicates are completely destroyed before the inflow reaches the radial distance labeled "4."

both compositions are distributed in size as a power law proportional to $a^{-3.5}$ between the minimum, a_-, and maximum, a_+, grain sizes. In determining the grain abundances at the outer boundary we assumed that all grains and the gas have the same inflow speeds. As inflow proceeds, the larger silicate grains slow down relative to the gas, and this causes the abundances of the larger silicate grain sizes to increase by ~45%. Shown is the silicate distribution from a point at the start of the steep velocity decrease. The original small-size silicate grains are destroyed, but grains of moderate size have decreased in radius to take their place. The largest silicate grains are too cool to suffer appreciable sublimation, and their relative grain to gas speeds cause their abundances to increase slightly. The change in the graphite distribution from that at the outer boundary to this location in the flow is negligibly small and has therefore not been plotted. Also shown are the distributions just prior to the destruction of the silicates and just prior to the destruction of graphites. The largest silicate grains remain relatively unchanged until they are finally destroyed by sublimation. The drift velocities of the largest graphite grains, however, cause their number abundances to increase by about a factor of 5. We conclude that the grain distribution at the shell's inner edge is much different than the distribution at the outer boundary. The number of small grains is greatly diminished, while the large grain population may even increase because of their slower infall speeds.

e) Very Large Grains

Thus far we have considered conditions for star formation that require decreases in the sizes of grains relative to the MRN mixture. An alternative solution is also possible. Consider the coagulation of grains at the outer boundary of the cloud. Let us assume that the coagulation does not change the gas-to-dust mass ratio and the size distribution remains proportional to $a^{-3.5}$. If the initial grains are very large, then infall will not be impeded because the outward radiative force tends to be proportional to $\int n(a)a^2 da$, and, while the grain area increases with grain radius as a^2, the grain abundance decreases as $a^{-3.5}$. Two constraints on our large grain population must be satisfied to allow infall. The first constraint requires that the outward radiative acceleration on the gas due to the collection of grains must be less than the inward gravitational acceleration. This constraint for the case of decreasing grain sizes was discussed in § V ($\Gamma < 1$, eq. [10]). The second constraint requires that the large grains be flowing inward relative to the central star. An outward motion of grains tends to increase the dust density due to a "snow plow" effect and eventually halts the accretion flow (Yorke 1980). The outward grain motion led to the end of the accretion phase for the 10 $M_\odot$ model calculated by Yorke. As we shall see, this second constraint imposes a more stringent limitation on the size of large grains.

Let us first discuss the effects on the radiation pressure opacity per gram of gas $\kappa_H^{\rm pr}$, resulting from grain coagulation. The opacity from the ensemble of grains is a function of the grain cross section, $C_H^{\rm pr} = \pi a^2 Q_H^{\rm pr}$, integrated over all sizes:

$$\kappa_H^{\rm pr} \propto \int_{a_-^i}^{a_+^i} A_i a^{-3.5} \pi a^2 Q_H^{\rm pr} da \,, \tag{39}$$

where A_i is the scale factor for material of composition i. To evaluate equation (39) we need to know the limits of integration a_-^i, a_+^i, and the behavior of $Q_H^{\rm pr}$ with grain size. The limits of integration are obtained from the requirement that the grain-to-gas mass ratio remain constant as grains grow:

$$\frac{M_{\rm grain}^i}{M_{\rm gas}} = \int_{a_-^i}^{a_+^i} A_i a^{-3.5} \frac{4}{3} \pi a^3 \rho_i da \frac{X}{m_{\rm H}} = \text{constant} \,, \tag{40}$$

where ρ_i is the density of grain material i. This condition can be expressed simply in terms of the minimum and maximum grain radii:

$$a_+^{1/2} - a_-^{1/2} = \text{constant} \,. \tag{41}$$

For an initial MRN distribution the "constant" = $(0.25\ \mu\text{m})^{1/2} - (0.005\ \mu\text{m})^{1/2} = 4.29 \times 10^{-1}$.

Next consider the behavior of $Q_H^{\rm pr}$ with grain size and its effect on the opacity $\kappa_H^{\rm pr}$. In the Rayleigh limit ($a \ll \lambda/2\pi$) the efficiency increases linearly with grain radius, and we see from equations (39) and (41) that the radiation pressure opacity remains constant. For larger grains ($a \approx \lambda/2\pi$) the efficiency increases with grain radius faster than $a^{1.0}$ and grain growth increases $\kappa_H^{\rm pr}$. This is the case for initial clumping of the MRN distribution in a $T_{\rm rad} = 1000$ K radiation field. The efficiency increases with a until $a \gg \lambda/2\pi$, beyond which $Q_H^{\rm pr} \approx 1$ (assuming $Q^S \approx Q^4 \approx 1$ and $g \approx 1$). Equations (39) and (41) show that further increases in grain size decreases $\kappa_H^{\rm pr}$ due to the steep dependence of grain abundance with grain radius ($\propto a^{-3.5}$). We find we can satisfy the outer boundary constraint of § V for the case of accretion onto a 100 $M_\odot$ core, $\dot{M} = 1 \times 10^{-3}\ M_\odot\ \text{yr}^{-1}$, at $T_{\rm rad} = 1000$ K using the DL abundances and $a_+^{\rm C} = 18\ \mu$m, $a_+^{\rm Si} = 18\ \mu$m.

We now discuss our second constraint, viz., that grains must flow inward relative to the central star. Using equations (32) and (33) (here the thermal terms can safely be ignored) and the

$\dot{M} = 1 \times 10^{-3}$ yr^{-1} model parameters from Table 1, we find the $a = 18$ μm grains are blown *outward* and would therefore halt the accretion flow, even though the opacity from the collection of grains, κ_H^{pr}, is low enough to allow $\Gamma < 1$. We note, however, that the gravitational force on a grain is proportional to a^3, so that by further grain growth the inward pull of gravity plus collisional drag can become larger than the outward radiative force. The minimal size grain, a_{min}, for this to occur is found using the grain equation of motion (eq. [22]), and the assumption that grains move at their terminal velocity

$$a_{min} = \frac{L}{c} - |u|\dot{M}\Big/\frac{16}{3}\pi\rho_i GM , \qquad (42)$$

where Q_H^{pr} is of order unity. Table 4 lists a_{min} for several accretion rates. We conclude that for the inward flow of both gas and grains the radius of a refractory grain would have to be larger than 100 μm. Since we believe this grain size is rather large, we prefer the modifications of the MRN grain distribution that decrease the grain sizes as disucssed in the previous sections. It is interesting, nevertheless, to note that accretion is allowed either for the case of very small or for very large grains but not for grains of intermediate sizes. To produce either just large or small grains would require some sort of preconditioning of the protostellar cloud.

f) Additional Core Mass Models

In this section results for models of 60 $M_\odot$ and 200 $M_\odot$ cores are presented, and some general trends in the relative importance of grain destruction processes are discussed. Table 3 lists parameters and results for all three core masses considered. As expected, the 200 $M_\odot$ core requires a higher rate of mass inflow than the lower mass cores and the initial grain sizes and abundances decrease with increasing core mass.

The ratio of the rate of sublimation to surface reactions, χ_{sub}, is also shown in Table 3, where we evaluate the destruction rates for the largest graphite grain at the point in the flow where 90%–95% of the mass of the grain has been removed. Also shown is the value of the drift-to-gas speed ratio, $|v_d/u|$. A value of $|v_d/u| = 1$ means the grain is stationary with respect to the central star. Note that the ratio of the rate of sublimation to surface reactions decreases for the highest core masses; that is, sublimation dominates grain destruction for the 60 $M_\odot$ core, but surface reactions are comparable to sublimation for the 100 and 200 $M_\odot$ cores. This is because the grain temperatures for the higher mass cores are much too low for sublimation to dominate the grain destruction processes. This decrease in temperature with increasing core mass can be understood by comparing the $|v_d/u|$ ratios. We see that grains are nearly brought to a halt in the 200 $M_\odot$ model. Because of the slow infall speed, the grain abundances rapidly increase at the inner boundary, thereby shielding grains farther out from heating by the stellar radiation field. Grains therefore remain cooler in the higher mass models until the edge of the shell where grain temperatures rapidly increase to similar values for all three core masses considered.

We also see that the lower grain temperatures produce overall lower destruction rates. However, even with the reduced rates, grains are destroyed at a larger distance from the central star for the higher mass cores. This increase in r_1 is a result of two effects. First, the larger luminosities can simply heat grains to destruction temperatures at larger distances from the core. Second, the slow grain infall speeds, found in the massive core models, increase the grain travel time. Therefore, grains are destroyed at larger distances even though the destruction rates are much lower.

TABLE 4

MINIMUM GRAIN SIZE IN GEOMETRIC LIMIT: CORE MASS = 100 $M_\odot$

$\dot{M}$ ($M_\odot$ yr^{-1})	log L_{tot}[a] ($L_\odot$)	M_{tot}[b] ($M_\odot$)	u[c] (km s^{-1})	a_{min}[d] (μm)
5×10^{-3}.....	6.386	3.85×10^2	3.46	1.04×10^3
1×10^{-2}.....	6.548	7.21×10^2	4.18	5.17×10^2
2×10^{-2}.....	6.759	1.40×10^3	5.15	1.19×10^2

[a] Total core plus shock luminosity.
[b] Total core plus shell mass.
[c] Free-fall inflow speed onto M_{tot}.
[d] Minimum inflowing grain size assuming composition is graphite, $\rho = 2.26$ g cm^{-3}.

VIII. SUMMARY AND CONCLUSIONS

Our investigation of the conditions necessary for the formation of massive stars is summarized as follows:

1. From a consideration of the radiative versus gravitational accelerations at the outer boundary of a protostellar accretion flow (§ V*a*) we have found the minimum modifications to the standard MRN diffuse cloud grain mixture that will allow massive stars to form. The largest graphite grain size must be reduced to 0.05 μm, which is 0.2 times the maximum size in the MRN mixture. The overall abundances must be reduced to one-fourth of the standard Galactic values as determined by DL. Clearly major modifications of a MRN mixture of grains is necessary before massive star formation will occur.

2. Considering the momentum flux at the inner boundary of the dust shell (§ V*b*), we find that inflow rates must be larger than 10^{-3} $M_\odot$ yr^{-1}. A protostellar cloud with initial turbulence greater than 3 km s^{-1} could possibly produce such a high rate of mass inflow.

3. From our detailed modeling we find that the radiative deceleration of the flow imposes additional constraints on the grain size, abundance, and mass inflow rate. A 100 $M_\odot$ core can continue accreting its surrounding envelope if the maximum graphite and silicate grain sizes are $a_+^C = 0.02$ μm and $a_+^{Si} = 0.2$ μm and the overall abundances decreased to one-eighth of the standard Galactic value. The inflow rate is 5×10^{-3} $M_\odot$ yr^{-1}. Note that although we must reduce the graphite abundance to allow inflow, we cannot eliminate it completely. This is because we need a material that will allow the inflow to accelerate to high speeds before absorbing the UV and visible radiation from the core. Silicates alone are destroyed at too large a radial distance and cannot shield the inflowing material.

These findings seem to support the theory of shock-induced star formation (Elmegreen and Lada 1977). An external shock produced by a supernova (Assousa and Herbst 1980), spiral density wave (Woodward 1976), or ionization front (Elmegreen and Lada 1977) from a nearby stellar association may modify the grains and produce the conditions suitable for massive star formation.

Alternatively, rotating infall may relieve some constraints imposed by spherical accretion. In this picture, the infrared radiative forces may not impede material flowing radially through an optically thick disk. Also the luminosity from accretion may be less than that in the spherical case (see Adams

and Shu 1986). However, it is not clear that infall directly onto a disk can be maintained unless the disk shadows infalling dusty material from a large fraction of the ultraviolet and visible radiation emitted by the core. Furthermore, the accretion luminosity remains low only for inefficient processing of material through the disk. Such a low efficiency builds up massive disks which may be unstable to fragmentation (Cassen *et al.* 1981).

There are several well-studied regions that are excellent candidates for star formation by external triggering. A recent analysis of the velocity structure of the W3 molecular cloud by Thronson, Lada, and Hewagama (1985) indicates that star formation was induced by the expanding W4 ionization front. Also, the turbulent velocities found in the star-forming layer are high enough that if gravitational collapse occurs, it must have large rates of mass inflow. We note that this region is certainly producing massive stars since W3 IRS5 is one of the most luminous Galactic IR compact objects known.

The 30 Doradus region in the LMC may be located at the point where a number of H I shells overlap (Canto *et al.* 1980). These giant shells (>1000 pc) are driven by massive OB associations. The dust-to-gas ratio is also observed to be decreased by at least a factor of 4 from the Galactic value (Koornneef 1985). Additional modification of the grain distribution by the expanding shells may have satisfied our conditions for very massive star formation in the 30 Dor region. Further study of grain destruction at molecular cloud boundaries must be examined to see if the required grain distribution can be produced.

We thank J. Mathis, E. Churchwell, P. Cassen, F. Shu, and D. Massa for helpful comments and suggestions. D. Cox was helpful in deriving the proof for the grain continuity equation. The calculations were carried out at the MADRAF computer facility at the University of Wisconsin-Madison. This research was supported in part by NASA grant NAGW-283.

APPENDIX A

OUTER BOUNDARY AND ESTIMATE OF MASS CONTAINED WITHIN SHELL

From the gas equation of motion we have

$$u(r)^2 = \left[u(r_2)^2 - \int_{r_2}^{r} \frac{2GM(r)}{r^2}\, dr \right]. \tag{A1}$$

Substituting the expression for $M(r)$, equation (12), into equation (A1) we find

$$u(r)^2 = \left\{ u(r_2)^2 - \int_{r_2}^{r} \frac{2G}{r^2} \left[M_* + \dot{M} \int_{r_1}^{r} \frac{dr}{|u(r)|} \right] \right\}. \tag{A2}$$

Using the gas continuity equation (11) and assuming that $u(r_2)$ equals the free-fall velocity onto the total core plus shell mass, i.e., $M(r_2) = M_* + M_{\rm shell}$, the density at r is

$$\rho(r) = \frac{\dot{M}}{4\pi r^2} \left\{ \frac{2GM(r_2)}{r_2} - \int_{r_2}^{r} \frac{2G}{r^2} \left[M_* + 4\pi \int_{r_1}^{r} r^2 \rho(r) dr \right] \right\}^{1/2}. \tag{A3}$$

An iterative loop to find $M(r)$ is as follows:

1. Pick the initial r_2 to be the radius at which the gas density flowing onto the core mass alone is 10^{-19} g cm^{-3}:

$$r_2 = \left[\frac{\dot{M}}{4\pi(10^{-19})(2GM_*)^{1/2}} \right]^{2/3}. \tag{A4}$$

2. We approximate the density as

$$\rho(r) = \frac{\dot{M}}{4\pi(2GM_*)^{1/2} r^{3/2}}. \tag{A5}$$

3. Carry out the integral in equation (A3) to obtain a new estimate for $\rho(r)$.
4. Find a shell mass, and thus $M(r_2)$, from

$$M_{\rm shell} = 4\pi \int_{r_1}^{r_2} r^2 \rho(r) dr. \tag{A6}$$

5. Repeat steps (3) and (4) until the density distribution is converged.
6. The density at r_2 is no longer equal to 10^{-19} g cm^{-3} because of the additional contribution of the shell mass in calculating $u(r_2)$. Using the gas continuity equation (11), estimate a new outer boundary, r_2':

$$r_2' = \left\{ \frac{\dot{M}}{4\pi[2GM(r_2)]^{1/2} 10^{-19}} \right\}^{2/3}. \tag{A7}$$

Since the outer boundary point has moved, we must redefine our radial grid to begin at the new r_2'. Repeat the density iteration.

7. Iterate between step (2) and step (6) until both the outer boundary, r_2, and density grid are converged.

APPENDIX B

GRAIN CONTINUITY EQUATION

Consider a discrete continuity equation for the case of fixed bin edges. Let $n_j(r, t)$ equal the total number density of grains within bin j and $\tilde{n}_j(a, r, t)$ equal the normalized distribution of grains within the bin. Then

$$n(a, r, t) = n_j(r, t)\tilde{n}_j(a, r, t) \tag{B1}$$

is the number density of grains at radius r and time t with grain size between a and $a + da$. Note that in the main part of this paper the grain abundance has units of number of grains per hydrogen atom in the range a to $a + da$. To convert to a number density multiply the abundance by $X\rho/m_{\rm H}$, where X is the mass fraction of hydrogen. The continuity equation for bin j is

$$\frac{\partial n_j}{\partial t} = -\frac{1}{r^2}\frac{\partial}{\partial r}(r^2 n_j w_j) + n_{j+1}\left[\tilde{n}\left(-\frac{da}{dt}\right)\right]_{a_j+1} - n_j\left[\tilde{n}\left(-\frac{da}{dt}\right)\right]_{a_j} - R_j n_j , \tag{B2}$$

where the second term on the right-hand side is the number of grains moving into n_j from n_{j+1} due to ablation, the third term is the number of grains moving out of n_j into n_{j-1} due to ablation, and the fourth term is the number of grains vanishing from n_j due to vaporization.

To obtain the continuity equation for a continuous distribution divide equation (B2) by $\Delta a = a_{j+1} - a_j$ and take the limit as $\Delta a \to 0$:

$$\frac{\partial n(a, r, t)}{\partial t} = -\frac{1}{r^2}\frac{\partial}{\partial r}[r^2 n(a, r, t)w(a, r, t)] - \frac{\partial}{\partial a}[n(a, r, t)\dot{a}] - Rn(a, r, t) . \tag{B3}$$

Consider the continuity equation for bins with variable boundaries. Let N_j equal the total number of grains within bin j:

$$N_j = \int_{a_j(t)}^{a_{j+1}(t)} n(a, r, t)da , \tag{B4}$$

where the limits of integration are functions of time. From Leibniz's rule

$$\frac{\partial N_j}{\partial t} = \int_{a_j(t)}^{a_{j+1}(t)} \frac{\partial}{\partial t} n(a, r, t)da + n(a, r, t)\dot{a}\Big|_{a_j(t)}^{a_{j+1}(t)} . \tag{B5}$$

Substituting equation (B3) into equation (B5), we have

$$\frac{\partial N_j}{\partial t} = -\frac{1}{r^2}\frac{\partial}{\partial r}\int_{a_j(t)}^{a_{j+1}(t)} r^2 n(a, r, t)w(a, r, t)da - n(a, r, t)\dot{a}\Big|_{a_j(t)}^{a_{j+1}(t)} - \int_{a_j(t)}^{a_{j+1}(t)} Rn(a, r, t)da + n(a, r, t)\dot{a}\Big|_{a_j(t)}^{a_{j+1}(t)} . \tag{B6}$$

Note that the second and fourth terms on the right-hand side cancel out. We define the average velocity and vaporization rates:

$$w_j = \int_{a_j}^{a_{j+}} n(a, r, t)w(a, r, t)da/N_j , \qquad R_j = \int_{a_j}^{a_{j+1}} Rn(a, r, t)da/N_j , \tag{B7}$$

and write the continuity equation (B6) as

$$\frac{\partial N_j}{\partial t} = -\frac{1}{r^2}\frac{\partial}{\partial t}(r^2 N_j w_j) - R_j N_j . \tag{B8}$$

Our numerical calculations use the simplest form for w_j, that is, $w(a, r, t)$ is not weighted by the grain number density across the bin: $n(a, r, t)$ equals a constant over a bin, and $w(a, r, t)$ is linear across a bin. The average velocity is then

$$w_j = \tfrac{1}{2}[w(a_j) + w(a_{j+1})] . \tag{B9}$$

To calculate the average vaporization rate over bin j, we need to discretize the vaporization rate for the continuous distribution. First, bin all grains that will not be contained within bin j. From equation (37) we have

$$n(a, r, t)R = n(a, r, t)\sum_k N_k f_T(v_{\rm rel})\sigma(a, \langle a\rangle_k)|w_k - w(a)| , \tag{B10}$$

where $\langle a\rangle_k$ is an average grain size over the bin and k is summed over all compositions and sizes. Next integrate the rate equation over grains that are contained within bin j. Substituting equations (B7) into equation (B10) we obtain

$$N_j R_j = N_j \sum_k N_k f_T(w_j, w_k)\sigma(\langle a\rangle_j, \langle a\rangle_k)|w_k - w_j| , \tag{B11}$$

where the threshold function, f_T is a function of the relative averaged bin velocities. In calculating the collision cross sections between bins the simplest average grain size is used:

$$\langle a\rangle_j = \tfrac{1}{2}(a_j + a_{j+1}) . \tag{B12}$$

Combining equations (B11) and (B8) and setting partial time derivatives equal to zero as appropriate for a steady-state accretion flow, we find

$$\frac{1}{r^2}\frac{d}{dr}(r^2 N_j w_j) = N_j \sum_k N_k f_T(w_j, w_k)\sigma(\langle a\rangle_j, \langle a\rangle_k)\,|w_k - w_j|\,. \tag{B13}$$

In terms of a discrete radial grid we finally obtain our grain continuity equation including vaporization:

$$r_{n+1}^2 w_{ij,n+1} N_{ij,n+1} = r_n w_{ij,n} N_{ij,n} \exp\left\{-\tfrac{1}{2}[(R_{ij,n}/w_{ij,n}) + (R_{ij,n+1}/w_{ij,n+1})](r_n - r_{n+1})\right\}, \tag{B14}$$

where the n and $n+1$ subscripts refer to decreasing radial distances in the inward integration.

REFERENCES

Adams, F. C., and Shu, F. H. 1986, *Ap. J.*, **308**, 836.
Appenzeller, I., and Tscharnuter, W. 1974, *Astr. Ap.*, **30**, 423.
Assousa, G. E., and Herbst, W. 1980, in *Giant Molecular Clouds in the Galaxy*, ed. P. M. Solomon, and M. G. Edmunds (New York: Pergamon), p. 275.
Barlow, M. J. 1978, *M.N.R.A.S.*, **183**, 367.
Barlow, M. J., and Silk, J. 1977, *Ap. J.*, **215**, 800.
Bodenheimer, P. 1983, *Lectures Appl. Math.*, **20**, 141.
Bodenheimer, P., and Sweigart, A. 1968, *Ap. J.*, **152**, 515.
Bohlin, R. C., Savage, B. D., and Drake, J. F. 1978, *Ap. J.*, **224**, 132.
Bohren, C. F., and Huffman, D. R. 1983, *Absorption and Scattering of Light by Small Particles* (New York: Wiley).
Boss, A. P. 1984, *Ap. J.*, **277**, 768.
———. 1985, *Icarus*, **61**, 3.
Burke, J. R., and Silk, J. 1976, *Ap. J.*, **210**, 341.
Canto, J., Elliott, K. H., Goudis, C., Johnson, P. G., Mason, D., and Meaborn, J. 1980, *Astr. Ap.*, **84**, 167.
Cassen, P. M., Smith, B. F., Miller, R. H., and Reynolds, R. T. 1981, *Icarus*, **48**, 377.
Cassinelli, J. P. 1979, *Ann. Rev. Astr. Ap.*, **17**, 275.
Castor, J. I. 1981, in *Physical Processes in Red Giants*, ed. I. Iben, and A. Renzini (Dordrecht: Reidel), p. 285.
Chu, Y.-H., Cassinelli, J. P., and Wolfire, M. G. 1984, *Ap. J.*, **283**, 560.
de Jager, C. 1980, *The Brightest Stars* (Dordrecht: Reidel).
Draine, B. T. 1979, *Ap. J.*, **230**, 106.
Draine, B. T., and Lee, H. M. 1984, *Ap. J.*, **285**, 89 (DL).
Draine, B. T., and Salpeter, E. E. 1979*a*, *Ap. J.*, **231**, 77.
———. 1979*b*, *Ap. J.*, **231**, 438.
Elmegreen, B. G., and Lada, C. J. 1977, *Ap. J.*, **214**, 725.
Feitzinger, J. V., Schlosser, W., Schmidt-Kaler, T., and Winkler, C. 1980, *Astr. Ap.*, **84**, 50.
Fitzpatrick, E. L., and Massa, D. 1987, in preparation.
Gilman, R. C. 1972, *Ap. J.*, **178**, 423.
Humphreys, R. M., and McElroy, D. B. 1984, *Ap. J.*, **284**, 565.
Iglesias, E. 1977, *Ap. J.*, **218**, 697.
Kahn, F. D. 1974, *Astr. Ap.*, **37**, 149.
Koornneef, J. 1982, *Astr. Ap.*, **107**, 247.
Krügel, E., and Walmsley, C. M. 1984, *Astr. Ap.*, **130**, 5.
Kwok, S. 1975, *Ap. J.*, **198**, 583.
Lamy, Ph. L. 1974, *Astr. Ap.*, **35**, 197.
Larson, R. B. 1969, *M.N.R.A.S.*, **145**, 271.
Larson, R. B., and Starrfield, S. 1971, *Astr. Ap.*, **13**, 190.
Leider, H. R., Krikorian, O. H., and Young, D. A. 1973, *Carbon*, **11**, 555.
Leung, C. M., Herbst, E., and Heubner, W. F. 1984, *Ap. J., Suppl.*, **56**, 231.
Maeder, A. 1980, *Astr. Ap.*, **92**, 101.
Mathis, J. S., Rumpl, W., and Nordsieck, K. H. 1977, *Ap. J.*, **217**, 425 (MRN).
Palmer, H. B., and Shelef, M. 1968, in *Chemistry and Physics of Carbon*, Vol. **4**, ed. P. L. Walker, Jr. (New York: Dekker), p. 85.
Salpeter, E. E. 1974, *Ap. J.*, **193**, 579.
———. 1977, *Ann. Rev. Astr. Ap.*, **15**, 267.
Savage, B. D., and Mathis, J. S. 1979, *Ann. Rev. Astr. Ap.*, **17**, 73.
Seab, C. G., and Shull, J. M. 1983, *Ap. J.*, **275**, 652.
Shu, F. H. 1977, *Ap. J.*, **214**, 488.
Shull, J. M. 1978, *Ap. J.*, **226**, 858.
Shull, J. M., and Van Steenberg, M. E. 1985, *Ap. J.*, **294**, 599.
Stahler, S. W., Shu, F. H., and Taam, R. E. 1980, *Ap. J.*, **241**, 637.
———. 1981, *Ap. J.*, **248**, 727.
Terebey, S., Shu, F. H., and Cassen, P. 1984, *Ap. J.*, **286**, 529.
Thronson, H. A., Lada, C. J., and Hewagama, T. 1985, *Ap. J.*, **297**, 662.
Tohline, J. E. 1980, *Ap. J.*, **235**, 866.
Utrobin, V. P. 1984, *Astr. Space Sci.*, **98**, 115.
Weigelt, G., and Baier, G. 1985, *Astr. Ap.*, **150**, L18.
Winkler, K.-H. A., and Newman, M. J. 1980, *Ap. J.*, **236**, 201.
Wolfire, M. G., and Cassinelli, J. P. 1986, *Ap. J.*, **310**, 207.
Woodward, P. R. 1976, *Ap. J.*, **207**, 484.
———. 1978, *Ann. Rev. Astr. Ap.*, **16**, 555.
Yorke, H. W. 1979, *Astr. Ap.*, **80**, 308.
———. 1980, *Astr. Ap.*, **85**, 215.
———. 1984, in *Workshop on Star Formation*, ed. R. D. Wolstencroft (Edinburgh: Royal Observatory), p. 63.
Yorke, H. W., and Krügel, E. 1977, *Astr. Ap.*, **54**, 183.
Zinnecker, H., and Tscharnuter, W. M. 1984, in *Workshop on Star Formation*, ed. R. D. Wolstencroft (Edinburgh: Royal Observatory), p. 38.

JOSEPH P. CASSINELLI: Department of Astronomy, University of Wisconsin, 475 North Charter Street, Madison, WI 53706

MARK G. WOLFIRE: NASA Ames Research Center, Mail Stop 245-3, Moffett Field, CA 94035